DYNAMIC EARTHQUAKE TRIGGERING POTENTIAL ACROSS EARTHSCOPE'S TRANSPORTABLE ARRAY

by

Lisa Mae Linville

A thesis submitted to the faculty of
The University of Utah
in partial fulfillment of the requirements for the degree of

Master of Science

in

Geophysics

Department of Geology and Geophysics

The University of Utah

August 2014

The University of Utah Graduate School

STATEMENT OF THESIS APPROVAL

The following faculty members served as the supervisory committee chair and members for the thesis of Lisa Mae Linville.

Dates at right indicate the members' approval of the thesis.

Kristine L. Pankow, Chair	05/1/2014 Date Approved
Keith D. Koper, Member	05/29/2014 Date Approved
Michael S. Thorne, Member	05/29/2014 Date Approved

The thesis has also been approved by John M. Bartley, Chair of the Department of Geology and Geophysics

and by David B. Kieda, Dean of The Graduate School.

ABSTRACT

The abundance of data from the Earthscope U.S. Transportable Array (TA) eliminates observational barriers such as data paucity and station sampling bias that have in the past hindered our understanding of the processes involved in dynamic triggering. The price of data abundance is that strategies must be developed to automate the systematic recovery of earthquake information. Optimized amplitude threshold detectors in the time-domain used to automate the process of earthquake detection with the TA data result in databases dominated by site-specific noise contributions. To increase the accuracy of detection databases, we develop a frequency-domain detection algorithm that employs spectral characteristics to distinguish earthquakes from other band-limited noise sources. This spectral filtering algorithm doubles the accuracy rate compared to time-domain methods. Despite the improvements in detection accuracy, we find that false detections in single-station pick databases still comprise a majority of all detections from the TA data. Leveraging frequency-domain processing techniques to develop array visualizations enables robust earthquake detection to magnitudes at or below M2. We use this array method to explore 18 global mainshocks (M>7) exhibiting the highest surface wave amplitudes during the TA deployment. Of the 18 mainshocks studied, none show strong evidence of instantaneous dynamic triggering and only one offers limited evidence for delayed dynamic triggering. These results suggest that prolific triggering in the U.S. is a rare phenomenon, requiring amplitudes outside the range observed here and/or that

additional conditions (fluids, tectonic environment, frequency, or duration of shaking) within the amplitude ranges explored here play a primary role in dynamic triggering.

This work is dedicated to my father.

TABLE OF CONTENTS

ABSTRACT iii

LIST OF FIGURES viii

ACKNOWLEDGMENTS ix

Chapters

1. INTRODUCTION 1

    1.1 Previous Dynamic Triggering Research 1
    1.2 Focus and Objectives 3

2. DATA 5

    2.1 Data Sources: Array Network Facility (ANF) Catalog 5
    2.2 Data Sources: Transportable Array Waveform Data 6

3. EARTHQUAKE DETECTION ALGORITHMS 7

    3.1 Method Justification 7
    3.2 Single-station Detection Algorithm 8
        3.2.1 Preprocessing and Short Time Fourier Transforms 9
        3.2.2 Noise Deconvolution 10
        3.2.3 Developing Detection Thresholds 11
        3.2.4 Performance and Review 14
    3.3 Array Processing for Earthquake Detection 15
        3.3.1 Method 15
        3.3.2 Choosing Band Range 16
        3.3.3 Distance Sorting 16
        3.2.4 Stacking 17
        3.3.5 Image Mapping 17
        3.3.6 Performance and Review 17

4. ALGORITHM IMPLEMENTATION ON GLOBAL MAINSHOCKS 29

4.1 Which Mainshocks to Use 29
4.2 Background Noise Levels Across the TA 30
4.3 Calculating Significant Rate Increases (95% and 99% levels) 31
4.4 Choosing Window Length 32
4.5 Four Day Windows 33
4.6 Instantaneous Triggering 33
4.7 Delayed Triggering 34
4.8 Summary of Identified Dynamic Triggering 35

5. DISCUSSION 43

5.1 Background Rates 43
5.2 On the Found Instances of Dynamic Triggering 44

6. CONCLUSIONS 47

6.1 Summary of Conclusions 47
6.2 Future Work 49

APPENDIX 51

REFERENCES 53

LIST OF FIGURES

3.1 STA/LTA Tuning Comparison 20

3.2 Number of False Detections for Japan, 2011 Mainshock 21

3.3 Antelope EV2 Picks from Band-limited Signals 22

3.4 Characteristic Spectral Content in Earthquakes 23

3.5 Energy Distributions 24

3.6 Importance of Ks Detection Threshold for TA Data 25

3.7 Successful Pick Discrimination Based on Spectral Character 26

3.8 Frequency Array Method 27

3.9 Single-station Earthquake Detection vs. Frequency Array Method 28

4.1 Median Array Amplitudes 37

4.2 Mainshock Locations and Types 38

4.3 Array Background Content (Earthquakes and Noise) 41

4.4 Earthquake vs. Single-station Detections (Active Array Summary) 42

ACKNOWLEDGMENTS

This work benefited significantly from discussion, suggestions, and support from a number of institutions and individuals. I would like to acknowledge directly the guidance and direction of my advisor and committee chair, Kristine Pankow, and the relentless inspiration and assistance provided by the other members of my committee, Keith Koper and Michael Thorne. In addition to my committee, this work would not have been possible without the collaboration of Debi Kilb and Aaron Velaso, both of whom participated significantly in all aspects of the work presented here.

I would also like to recognize the generous support and assistance from the staff at the University of Utah Seismograph Stations and the Department of Geology and Geophysics at the University of Utah. Additional support for this project was provided by the National Science Foundation grant EAR 1053343.

CHAPTER 1

INTRODUCTION

1.1 Previous Dynamic Triggering Research

Following the Landers (M7.3, 1992) earthquake in California, seismologists noticed that significant increases in seismicity levels sometimes follow large earthquakes, but at distances beyond the reach of the traditional aftershock zone (Hill et al., 1993; Prejean et al., 2004). In the near-field, the redistribution of static stresses resulting from slip along a fault can alter the stress states of nearby faults such that fault strength is exceeded and an earthquake occurs. Beyond several fault rupture lengths, static stress changes decay to levels well below low-level earth forcing such as lunar tides, and therefore, a different physical explanation is needed for far-field observations. Surface waves are able to carry large energy transients to far greater distances than 3D propagating body waves and are hypothesized to be the physical mechanism for triggering remote earthquakes (Freed, 2005; Hill, 2008). Understanding when and where aftershocks are likely to occur is a significant aspect of analysis and mitigation following large earthquakes. Accordingly, the potential for a worldwide aftershock zone, through dynamic triggering, necessitates an understanding of the driving parameters of this process.

In the past decade, observations linking large global earthquakes to increases in seismicity rates at distant locations have increased significantly and, notably, an increasing number of these observations make this link following a delay in the passage of the surface waves, from hours to weeks (Brodsky, 2006; Freed & Lin, 2010; Jugla, 2011). Abundant physical models have been proposed for both instantaneous (Belardinelli et al., 2003; Brodsky et al., 2003; Hill et al., 1993) and delayed dynamic triggering (Johnson et al., 2005; Manga & Brodsky, 2006; Parsons, 2005; Shelly et al., 2011). Additionally, studies have reported a range of driving mechanisms, including amplitude (Feltzer & Brodsky, 2006; Trugman, 2013; van der Elst & Brodsky, 2010; Wu et al., 2012;), frequency dependence (Brodsky & Prejean, 2005), and structural orientation (Gonzales & Velasco, 2011).

While it is clear that a significant number of questions remain unanswered regarding the underlying physics of dynamic triggering, it is also true that first order questions persist. Understanding whether dynamic triggering is a rare occurrence that requires highly specific conditions (Parsons et al., 2014), or a ubiquitous process that occurs independent of tectonic environment (Gomberg and Sherrod, 2014; Velasco et al., 2008) can offer guidance to this quickly evolving field.

With the current expanse of global coverage, our understanding of the fundamental processes involved in dynamic triggering is no longer necessarily limited by lack of observations. Indeed, one new challenge in the last decade has been to develop strategies for systematic processing of large datasets. The expectation is that these datasets can elevate our understanding of the behavior of earthquakes and the factors driving their occurrence, from guesswork to verifiable scientific understanding.

1.2 Focus and Objectives

The large array aperture and dense (70 km) station spacing make the Transportable Array (TA), a branch of the EarthScope project, one of the most significant seismic deployments in the U.S. to date. While this makes possible unprecedented opportunities for probing the crust, it also poses significant challenges related to data abundance and fidelity. The focus of the following work is to develop a framework within which detecting dynamically triggered earthquakes from the TA dataset is both viable and robust.

Two specific benefits of using the TA are high station density and grid spacing. High station density enables the recovery of events smaller in magnitude than are routinely reported in seismic event catalogs. Parsons et al. (2014) suggest that small earthquakes (smaller than M3) are preferentially triggered by transient stress perturbations from large earthquakes. This is one way to reconcile the rarity of dynamic triggering in earthquake catalogs with the expectation of ubiquity from other methods. Preferential triggering of smaller magnitudes is also supported by the observation that only very limited cases of moderate to large dynamically triggered earthquakes have been reported. Pollitz et al. (2012) offers the one notable exception to this in reporting a global increase in M>5 following the Sumatra, 2012 events. If dynamic triggering occurs preferentially in the smaller magnitudes, this assumption should be validated by observation.

The second advantage, grid spacing, allows us to probe for crustal responses from zones that are rarely scrutinized, owing to their assumed quiescence. There are several cases in which dynamically triggered events are reported in areas distinctly different from background seismicity (Pankow et al., 2004; Parsons et al., 2014). These observations, in

addition to the prospect of capturing observations capable of demonstrating true ubiquity, make these unexplored areas particularly valuable.

To summarize, the first main objective of this investigation is to develop new methods to efficiently process the preponderance of available data from the TA. The larger goal is to use the method on a global mainshock database to systematically evaluate the occurrence of dynamic triggering within range of the TA, especially: 1) in areas previously unscrutinized, 2) to levels below typical catalog values, and 3) with sufficient evidence that associated rate increases are nonrandom and above background variation.

CHAPTER 2

DATA SOURCES

2.1 Array Network Facility (ANF) Catalog

The TA spans the continental U.S. occupying roughly 6° longitude bins, or approximately the width of New Mexico, at any given time. Since the aim of this study is to observe the local crustal response following a large earthquake, we are concerned only with earthquakes local to the array. As an exploratory tool and a basis for comparison, we use the seismic event catalog produced through traditional network-based (Antelope) analysis for TA data by the Array Network Facility (ANF, http://anf.ucsd.edu/tools/events/). Once parsed, this catalog provides an unfiltered version of seismic events reported within the footprint of the array. This represents the highest resolution event catalog available for the U.S. and is a direct product of the waveform data publicly available from TA stations. By comparison, event catalogs such as the Advanced National Seismic System (ANSS) typically limit reporting to tectonic earthquakes. This distinction is important considering rates of seismic events related to energy extraction typically exceed the significant variation in tectonic rates by more than two times the standard deviation (Astiz et al., 2013).

2.2 Transportable Array Waveform Data

All waveform data used in this study are downloaded from the IRIS/DMC data repository and pushed into a local continuous waveform buffer (CWB), which is managed by the University of Utah Seismograph Stations (UUSS). For all time periods investigated (see section 3.2 for a discussion on determining mainshocks and sections 3.3 for determining time windows) all network code 'TA' data for vertical channels (unless text explicitly states additional channels are used) are stored in the local data repository. This allows more seamless interaction with the data through internal programs without requiring other communication methods such as the java-based IRIS webservices.

CHAPTER 3

DETECTION ALGORITHMS

3.1 Method Justification

Time-domain picking algorithms, as implemented in many regional networks (i.e., those using Earthworm or Antelope software) use a short-term average/long-term average (STA/LTA) filter for phase picking and generally rely on secondary binding programs to associate individual picks into legitimate seismic events (see review in Allen, 1978). This method is based on having a reasonable sized array wherein more than one station can be used to identify a coherent wave-front across the network. This method allows for a small number of false alarms and if properly tuned, a robust framework for earthquake detection. The most significant drawback to using detections on multiple stations to identify coherent signal is that smaller events will not generate sufficient radiated seismic energy to be detected and associated on the required number of stations. Moving away from catalog and network processing to more independent methods such as single-station detection resolves these dependencies; wherever there is a seismometer, a rate increase can be determined. The cost of this independence is the associated need to account for nonnegligible noise contributions that are not reflected in catalog event data.

Noise contributions are an inevitable part of single-station detection owing to the practical relationship between sensitivity (the number of false detections a system can reasonably permit) and resolution (the lowest magnitudes recoverable). The performance of amplitude threshold detectors (STA/LTA detectors) is thus highly dependent on tuning (Figure 3.1). Even so, analysis of results from the Antelope EV2 detector optimally tuned for local earthquake detection on datasets for the Chile (2/27/2010, M8.8) and Japan (3/11/2011 M9.0) events demonstrates that array-wide detections are more reflective of noise local to each site rather than earthquakes (Figure 3.2).

False detections from the amplitude threshold detectors described above can often be the result of high amplitude signals within limited frequency bands (Figure 3.3). Conversely, earthquakes generate high amplitude signal at a broad range of frequencies, suggesting that amplitude threshold detection using spectral constraints can successfully increase the accuracy of single-station detection algorithms (Figure 3.4). Increased accuracy is a mandatory part of identifying statistically meaningful increases in tectonic events across the TA because these increases will otherwise be too subtle to resolve. The following sections in this chapter outline the development of exploratory methods based on frequency-domain earthquake detection for both single-station and array approaches.

3.2 Single-station Detection Algorithm

The basis of single-station detection in the frequency-domain is that by limiting picks to signals that include significant contributions above the background level from a broad range of frequencies, spurious high frequency detections can be avoided and the overall number of false picks in each station database reduced. For this method, 3 hours

of post-mainshock continuous waveform data is considered for 3 mainshock events; Chile (2/27/2010, M8.8), Japan (3/11/2011, M9.0), and Baja (4/11/2010, M7.9). Processing steps are outlined below.

3.2.1 Preprocessing and Short-Time Fourier Transform

Each mainshock is recorded by between 300-450 active TA stations. To begin, 3 hours of continuous waveform data is pulled from the UUSS CWB. To remove the obscuring long periods associated with the surface waves from each mainshock the traces are highpass filtered using Seismic Analysis Code (SAC) at 5 Hz (hp n 4 p 1 c 5), the mean and trend are removed, and the ends are tapered to avoid edge effects during subsequent transforms. Using the data from each station, x(n), where n is the number of samples each representing ground velocity, we divide into overlapping segments specified by a window length and type, w(n). For each segment, the discrete Fourier transform is computed. This short-time Fourier transform (STFT) remaps the input as a 3-dimensional signal with time, frequency, and amplitude parameters. The resultant output is compiled into a matrix (referenced as the B matrix in following text), which represents an estimate of the frequency content at a series of discrete time-steps for a vector of frequencies (zero-to-nyquist).

$$STFT\{x[n]\}(m,\omega) = \sum_{n=1}^{N} x[n]\omega[n-m]e^{-i\omega n} \tag{3.1}$$

For these short (3 hour) samples, we used a Hanning window length of 2^8 with an overlap of 2^7 (typically done to reduce spectral leakage, using the ideal overlap for Hanning at 50%, Heinzel et al., 2002).

3.2.2 Noise Deconvolution

Because we wish to analyze only transient signals, such as earthquakes, we explicitly remove the stationary signal systematically from every record. To accomplish this, we normalize each array value by the median signal amplitude at each frequency increment (index *i* in our notation, *j* index corresponds to time),

$$B(white)_{i,j} = \frac{B_{i,j} * n}{\sum_{i=1}^{n-1} B_i} \tag{3.2}$$

where n is the number of discrete time samples along each row. Taking the median has essentially the same result as taking the mean after removing the outliers using the Thompson Tau method (Ripley, 1989), but is significantly faster.

Throughout our code, and especially noteworthy when determining threshold values, we opted to use the median of our distributions because this value is considerably less sensitive to outliers and computationally more efficient than explicitly removing them (Leys et al., 2013, Figure 3.5). By normalizing the values for each entry within our frequency vector, we are able to distill the remaining information down to relevant analyzable content. In most cases, the resulting spectrogram offers a clear picture of the variation with minimal loss of relevant content.

This process is successful because, although over the length of the observational window, an individual trace may experience significant variation within a single frequency bin, the overall scale of the input is short compared to the temporal variation in background levels. In later tests, as the observation window is pushed to greater lengths (4 days), although not necessary, it became useful to introduce a level of sophistication into the noise deconvolution, namely, the normalizing values became a function of

distance along the time vector. This method allowed us to remove signals longer than typical earthquake duration for each record and results in significantly less background noise. Independent of static or dynamic noise normalization, the resulting matrix represents the time-localized values above the local noise level for each site over a range of frequencies between 0 and the nyquist frequency (1/2 the sample rate, or 20 Hz).

3.2.3 Developing Detection Thresholds

Detections are based on three frequency-stacked time-series. This is accomplished by summing the amplitudes over a limited range of frequencies and represents a time-series of the band-limited power estimate for each trace. We calculate one empirical threshold from each series. The first (k, 4-12 Hz) is used to verify that signals of interest sustain high power over a wide range of midband frequencies. The lowest (ks, 3-7 Hz) is to ensure at least some component of that energy is contained within the lower frequencies, and the highest (kh, 11-20 Hz) ensures a high-frequency contribution. This ratio was developed following the observation that some instrumental or ambient noise sources can be semibroadband without extending into the lower or higher frequencies, while for earthquakes, this is generally not true; most events contain at least a minimum amount of power in these ranges (Figure 3.6). Theoretically, this introduces a limit on the smallest magnitudes we are able to recover. Very small earthquakes are poor generators of low frequency energy. Conversely, there exists a class of low frequency earthquakes which, unless sizeable, these thresholds will exclude. In the implementation of any algorithm, there exists a balance between resolution and accuracy. Understanding this, we

choose to maintain a higher magnitude of completeness for the process and therefore also a higher level of confidence in the fidelity of our detections.

For short records (< 3 hours), it is suitable to use static threshold values in which the main threshold (k) is calculated based on signal median. Ks and kh are similarly determined but explicitly exclude portions of the trace that do not represent relevant contributions to local detection (the tapered tails and low frequency contributions coincident with the mainshock where the timing is predicted using TauP, http://www.seis.sc.edu/taup/). This method is successful when tested on records for an earthquake swarm in Yellowstone National Park. For these cases, threshold values can be many times greater than the standard deviation while still reliably capturing events below magnitude 1.

For longer records and because the TA dataset contains a more challenging noise distribution than typical regional networks, the detections in this study are based on the basic STA/LTA concept. As implemented here, the threshold values are determined from a running mean within a window prior to the index sample. Similar to tuning STA/LTA pickers in the time-domain, window length matters. By setting our window too short, we loose a realistic baseline. Windows too long make excluding protracted increases in signal strength very difficult. This issue becomes doubly important when we consider the time period coincident with the incoming energy from a distant mainshock in the low frequency bands. There is a specific window around the mainshock within which we do not escape the decay envelope for often greater than 10 minutes and therefore, this period is especially susceptible to false detections if set too low, and misses detections if set too high. Because understanding the time delay of dynamic triggering following a transient

stress perturbation is important for unraveling the underlying physical processes, signals within this time period are especially valuable, albeit the most difficult to detect. Empirical windows for threshold detection are related to the STFT window parameters and are on the order of tens of seconds in length (LTA) and define a threshold at 2.9, 2.9, and 3.5 above the median of k, ks, and kh, respectively.

The stacked time-series is then converted into a binary signal, based on whether it meets the criteria of being at or above all detection thresholds within a given time-step. For a typical tectonic earthquake, if the fft window is short compared to the duration of the earthquake, there will be a large number of swaps between time-steps coincident with the P and S wave phases and the amplitude decay will follow the decay envelope represented in the associated seismogram. In order to capture a unique detection from a single event, we sacrifice resolution in the time-domain, which merges values above k; in addition, we consider only the first entry from a run within the binary signal on all k values. We allow ks values to lag behind k values by up to three time-steps to allow for the later arrival of long period energy or precede it by one to allow for an apparent delay when the k threshold is high compared to the ks for that time window. We also require that a consecutive series of triggers drop below the k values within a 3-minute window to qualify as a detection. In the event that the threshold value k is exceeded every 512 samples over some duration (a 1, followed by a 0, followed by a 1, and so forth), the value in the middle is set to 1 (so that the string is 111) and therefore, only one detection will trigger. This eliminates the cases of a saw-type signal resulting in more than one detection. Amplitudes are additionally required to retain at least 15% of their value for the first three samples following a detection. This is aimed at eliminated detections from

telemetry drop-outs, which often produce high amplitude broadband spikes, which then return to background levels within one sample. In most cases this successfully yields one detection for each event with an approximate event time (Figure 3.7).

3.2.4 Performance and Review

An inescapable part of algorithm design is the inherent relationship between false detections and capture threshold. The optimal algorithm necessarily recovers the highest level of legitimate events, the lowest number of false picks, and includes events at a sufficiently low magnitude of completeness. For this study, we desire events smaller than catalog values can provide, thus $M < 2.0$. The basic time-domain STA/LTA, Antelope, and frequency-domain pickers operate on a continuum between brute force methods and highly selective, tuned algorithms. The basic STA/LTA end member will pick every high frequency signal just barely above the noise level; it will capture nearly 100% of events to a level of completeness equal to a trained analyst and in doing so, it will have typical false detection rates well above 98%. The performance of the Antelope EV2 detector reveals that even optimal tuning of STA/LTA time-domain algorithms do not result in robust event databases for TA stations. The frequency detector improved upon the false detection rate of the Antelope picker (5-10%), at very minimal cost to detection levels. Therefore, single-station detection databases for TA stations built with frequency detection will include a larger percentage of legitimate seismic events than those built with even optimally tuned traditional methods.

Implementation of the algorithm outlined above lowers the number of waveforms that require review (any with an earthquake detection) down to a process that is more

tractable. In a test case for the March, 2011 Japan earthquake, total detections decreased by more than 50%, while true pick counts remained the same, effectively doubling pick accuracy. Therefore, I submit that it provides a reliable and practical way of filtering the desired results from single records within a large data-set and represents a more reliable way of building pick databases than traditional time-domain methods.

3.3 Array Detection

Although increases in accuracy from the method outlined above are significant, array wide, they represent only a modest gain in eliminating noise sources as the dominant constituent. For any given mainshock, the false detection rates from frequency methods persist above 80% array wide. This remains problematic due to the non-stationary nature of background noise (for discussion on diurnal noise variation across TA, see section 4.2). Because one of our primary goals is to capture seismicity below catalog levels, it makes sense to leverage the frequency-domain processing techniques outlined above to include array processing. The objective for this is to drastically decrease the number of false detections by requiring energy fronts across the array to be coherent in order to be called an event. This is similar in principle to the association programs implemented in regional seismic networks.

3.3.1 Method

In section 3.2.3, the process of stacking the sum of the signal amplitude over a limited band is explained. This time-series is produced for each station and is the basis upon which single-station detections and thresholds are built. For array detections, we use

the same noise-limited amplitude stacks to build signal amplitude distribution visualizations for the active array through time. The process includes four steps: 1) Choosing a band range, 2) Sorting the stacks by distance based on a reference latitude or longitude, 3) Stacking each time-series to create an image, and 4) Saturating the image at a level which highlights the features of interest.

3.3.2 Choosing a Band Range

The direct control of frequency content for each stack allows the user to highlight specific features of interest. For example, in earthquake studies, the band range 4-12 Hz presents a clear picture of the desired frequencies for local seismicity. 4 Hz (rather than ~1 as is typical) is a reasonable low frequency cut-off because this limits contributions from long period energy high enough in amplitude to persist through the roll off in the high pass filter (5 Hz, 4 poles, 1 pass) as in the event of large amplitude surface waves from a temporally coincident global mainshock (e.g., dynamic triggering studies). In general, limiting the band range is a highly efficient way to display time-dependent signals and can be tuned for a number of elastic strain release phenomenon in the crust (e.g. tremor, cryostudies, VLF events, etc).

3.3.3 Distance Sorting

In order to visualize this multidimensional dataset in a single image, it is necessary to translate absolute spatial location to a relative distance via the formula:

$$dist_i = \sqrt{(A_i - A_{ref})^2 + (B_i - B_{ref})^2} \quad (3.1)$$

where A and B are the latitude and longitude positions for each station and the reference value is the closest station to the mainshock based on either latitude or longitude indexing.

3.3.4 Stacking

The summed amplitude values for each indexed station at each time-step determined during the STFT processing is looped into an array where the rows are the station, indexed by our distance vector, and the columns are time-steps. For an STFT window length of 2^8 and overlap of 5, you down-sample from 40 samples per second (sps) to .15 sps, or ~ 1 sample every 6 seconds. A window of 2^6 with the same overlap yields 1 sample every ~ 1.5 seconds.

3.3.5 Image Mapping

The stacked array is displayed as an image with pixel location corresponding to $row_{(i)}$, $column_{(j)}$, and each pixel hue determined by the normalized $B_{(i,j)}$ value (Figure 3.8). Typically, record glitches (most often associated with telemetry drop-outs and other electronic noise) exist in the records. If a static whitening process is used, saturating the pixel at a value within the range of the expected amplitude of your signal is mandatory. Empirically, for local earthquakes, this value is between 200–700 db.

3.3.6 Performance and Review

The image produced by the process outlined above presents us with a powerful tool for understanding how power distribution across the array changes through time. We

are able to robustly characterize seismic content from distance move-out based on logical seismic velocities. Additionally, characteristic noise patterns across the array become apparent as do specific low-quality data sites.

There are several notable limitations of this method. Timing resolution degrades according to the parameters of our frequency transformations. The price of this ultimately is that we are unable to pick specific wave phases and thus can no longer use event detections directly for earthquake location. We get around this by identifying the closest station to the epicenter based on first arrivals. Therefore, when determined, our earthquake centers are constrained to general regions rather than specific locations. Likewise, event origin times are limited by down-sampling constraints. Also, our distance criterion does not consider the location of the event a priori; therefore, the differential distance does not account for true spatial clustering. This is a sacrifice we make in exchange for visual efficiency; however, we recognize it is not a truly accurate portrayal of the 4-dimensional dataset. Lastly, unlike the methods discussed above for single-station detection, this method requires analyst review. The array image method is more analogous to picker/binder routines for seismic networks where temporally coincident picks get associated into events and then verified by an analyst. Unlike network routines, however, these detections are manual. This manual processing becomes more cumbersome the longer the input time for each image. If the image is not highly compressed (> 10 hours displayed in one frame), events demonstrating signal at 4 stations or more will be clearly identifiable. To demonstrate the potency of this method, we choose an hour of data from the Haida Gwaii, 2013 M7.8 mainshock and compare the number of events found in the ANF event catalog with the events our method detects for

the same time period. The ANF catalog contains 4 events where we recover 14. The 4 ANF events spatio-temporally correspond to the 4 largest events on our image. Further, if time-domain picks are mapped by the same method as our images, so that latitude, longitude, and time of the pick are related in the same way, and the two images are overlain, it becomes clear that if an event is reliably picked by single-station methods on at least 3 stations, it will be identified in our image on a number of stations >3 and therefore highly visible (Figure 3.9). For quantitative backing, we observe that only between 23-53% of stations out of the total number of stations demonstrating clear association respond with a detection. This means that with a mean pick rate of 35%, for every one earthquake detection from single-station methods, the array method will provide three. This demonstrates that our method is capable of robustly identifying seismicity across the array to a level much lower than any existing catalog and comparable to single-station detectors, the main difference being that the number of false picks we include in this high resolution seismicity database is *near zero*.

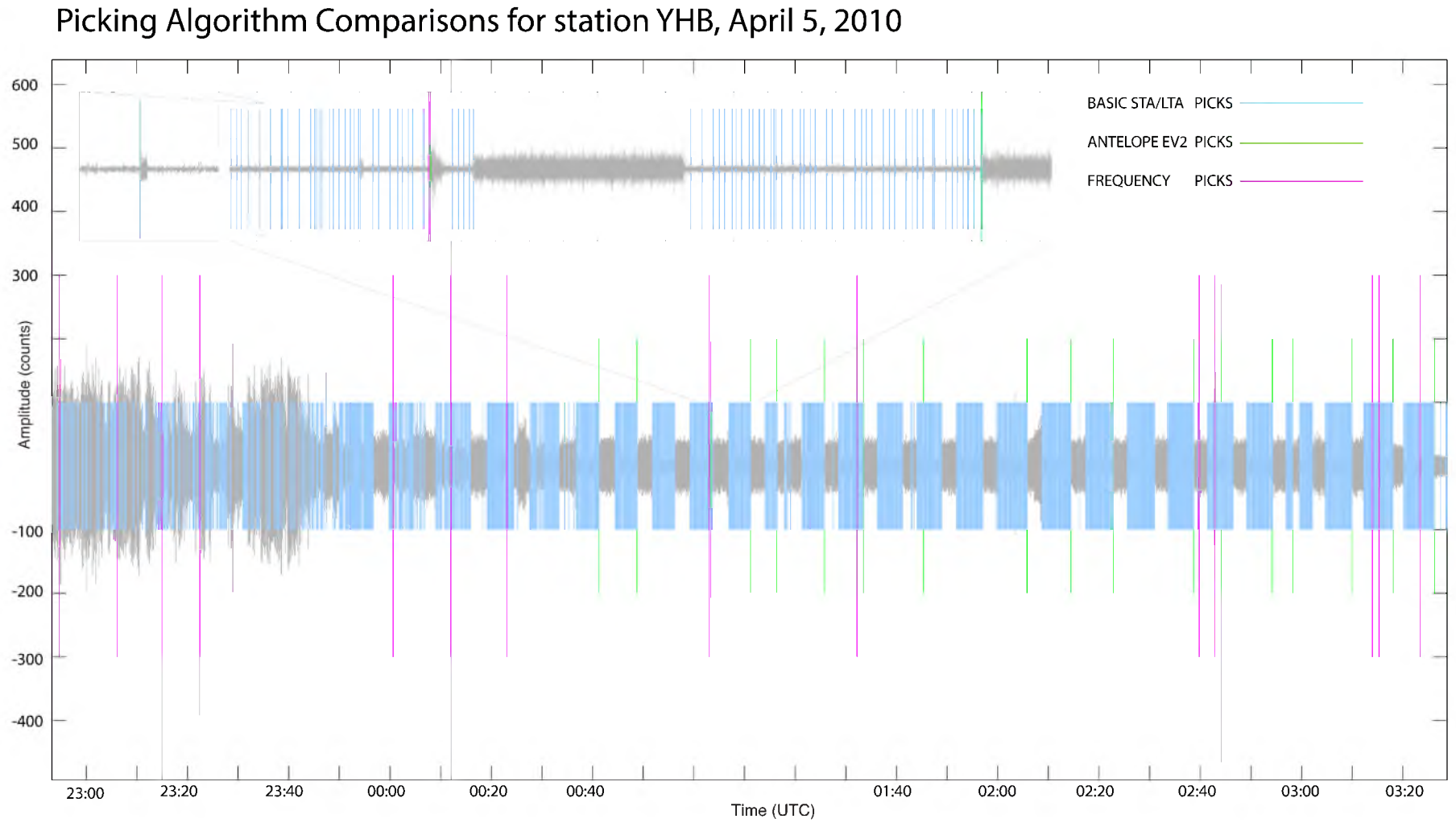

Figure 3.1 STA/LTA tuning differences. Blue represents a basic STA/LTA from the Earthworm distribution. Green picks are from the Antelope Ev2 detector tuned for TA data and the magenta lines are from a frequency-domain picking algorithm developed here. In the zoom panel (top) all algorithms pick on the small earthquake while the basic STA/LTA picks all signal increase and the antelope picks on the higher amplitude signal increases and the frequency method picks only the earthquake.

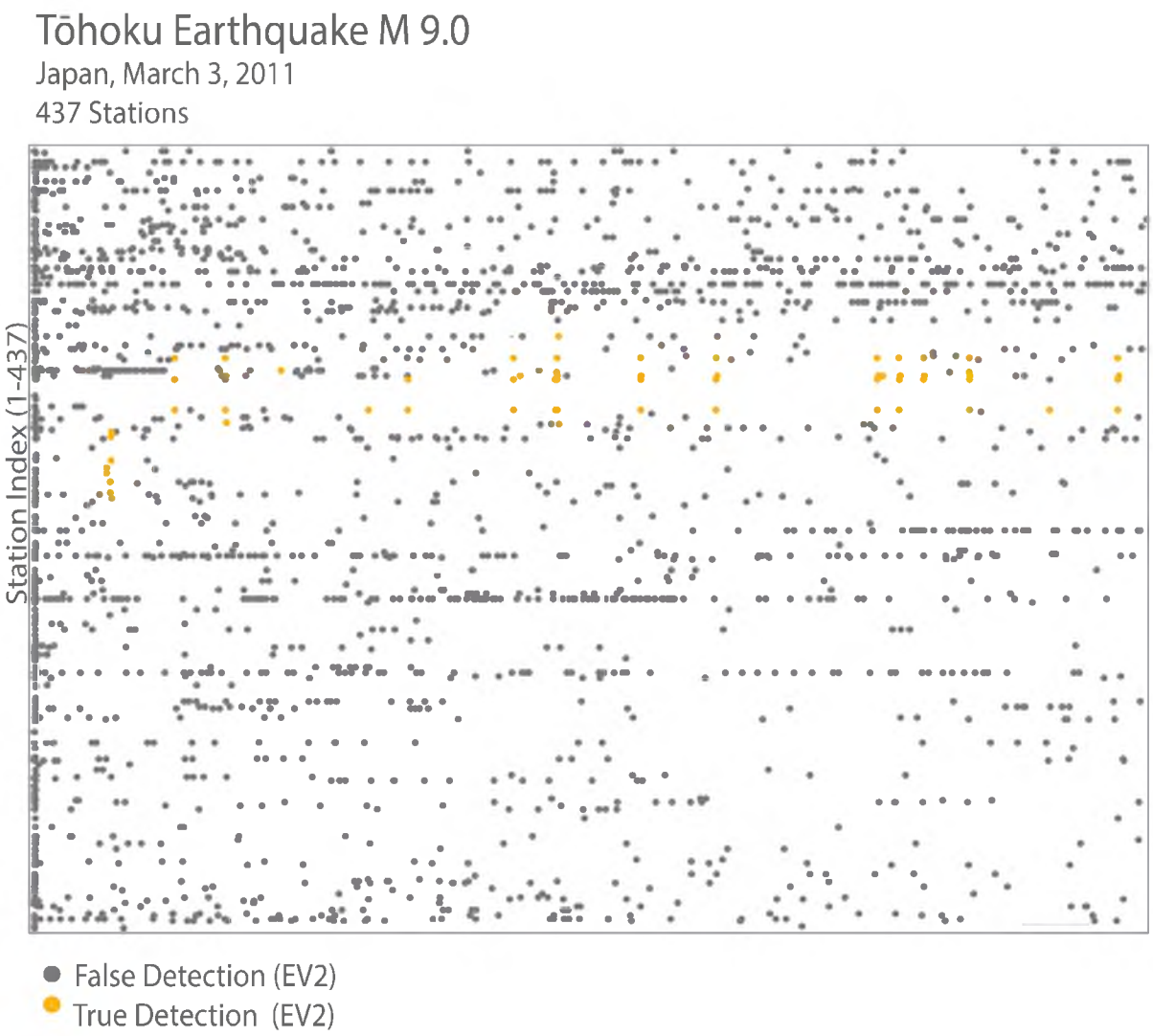

Figure 3.2 False vs. true detections for Tohoku, 2011 magnitude 9.0 earthquake. Array wide the percentage of false detections is very high (grey dots) compared to the number of true detections (gold dots)

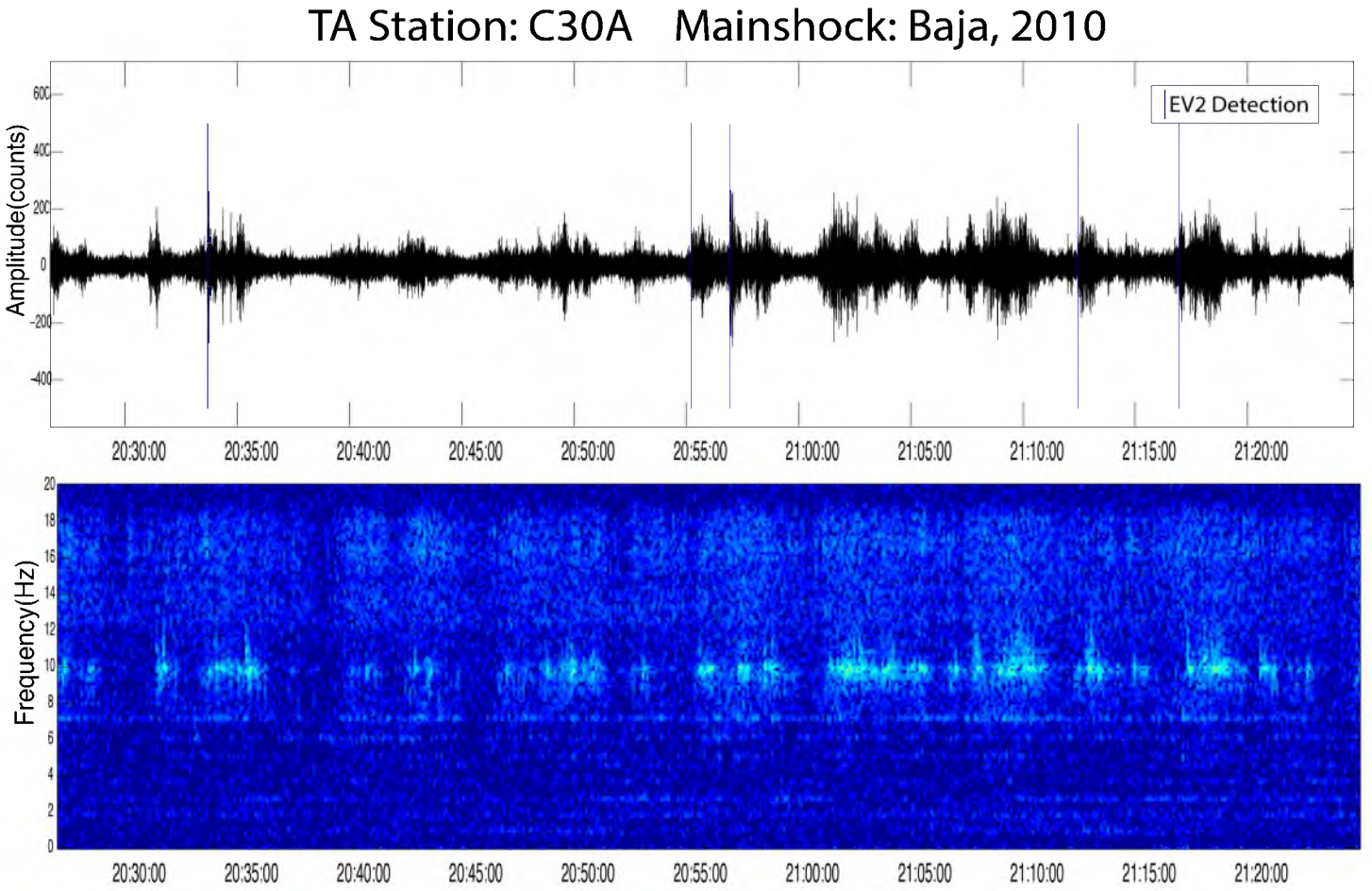

Figure 3.3 A significant number of false picks from the EV2 detector are the result of band-limited (between 8-12 Hz) noise sources.

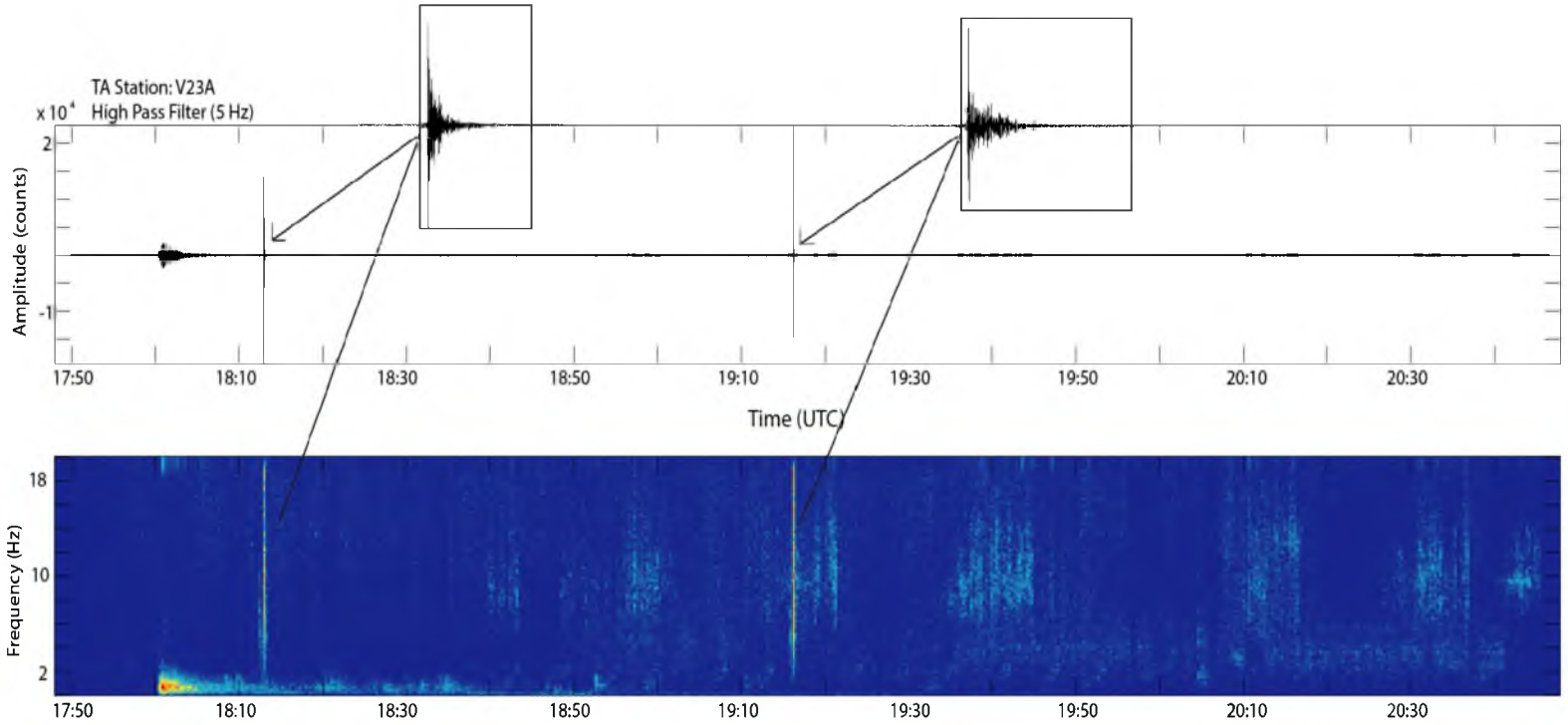

Figure 3.4 Two earthquakes in the spectrogram of station V23A are clearly visible as time-limited broadband signals.

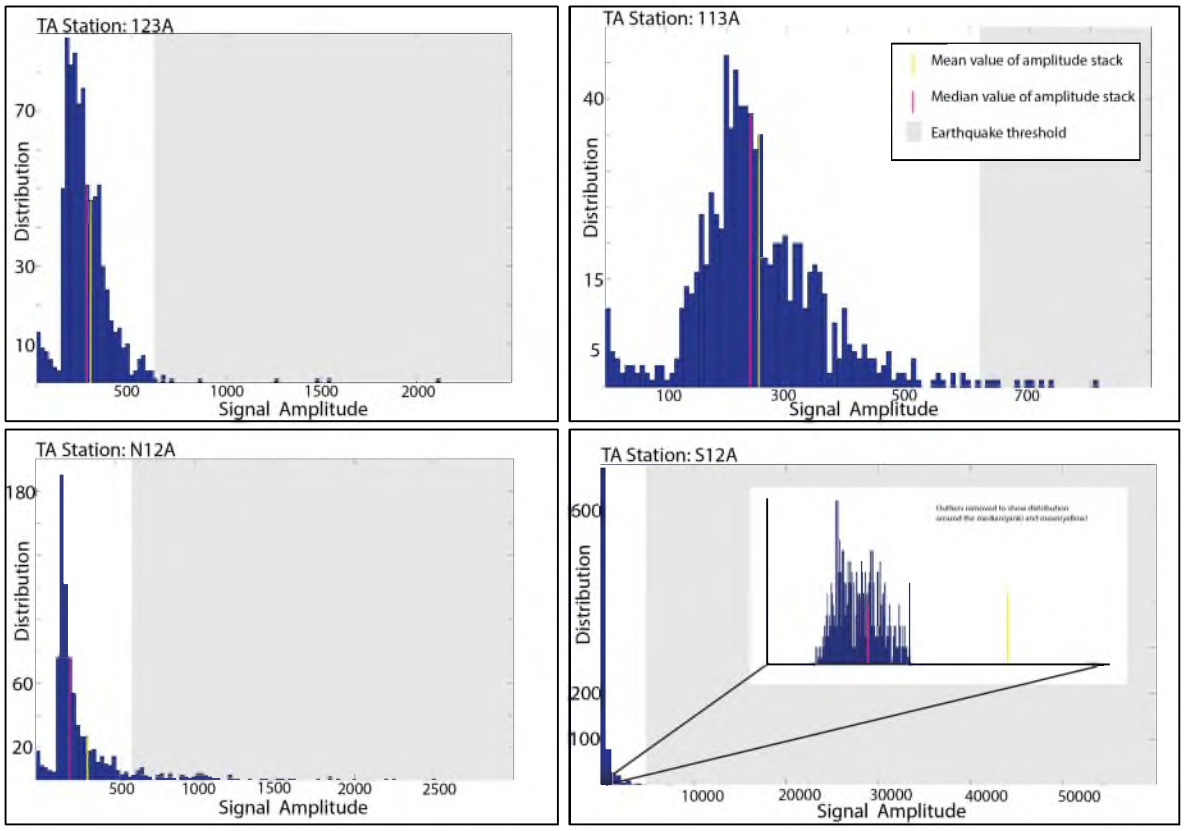

Figure 3.5 The effect of mean vs. median values for choosing static amplitude thresholds from signal amplitude distributions. The difference between these two values becomes the greatest, and therefore the most meaningful for earthquake detection, in the presence of extremely high signal amplitudes, such as from large local earthquakes. The shaded region indicates 2σ for each distribution.

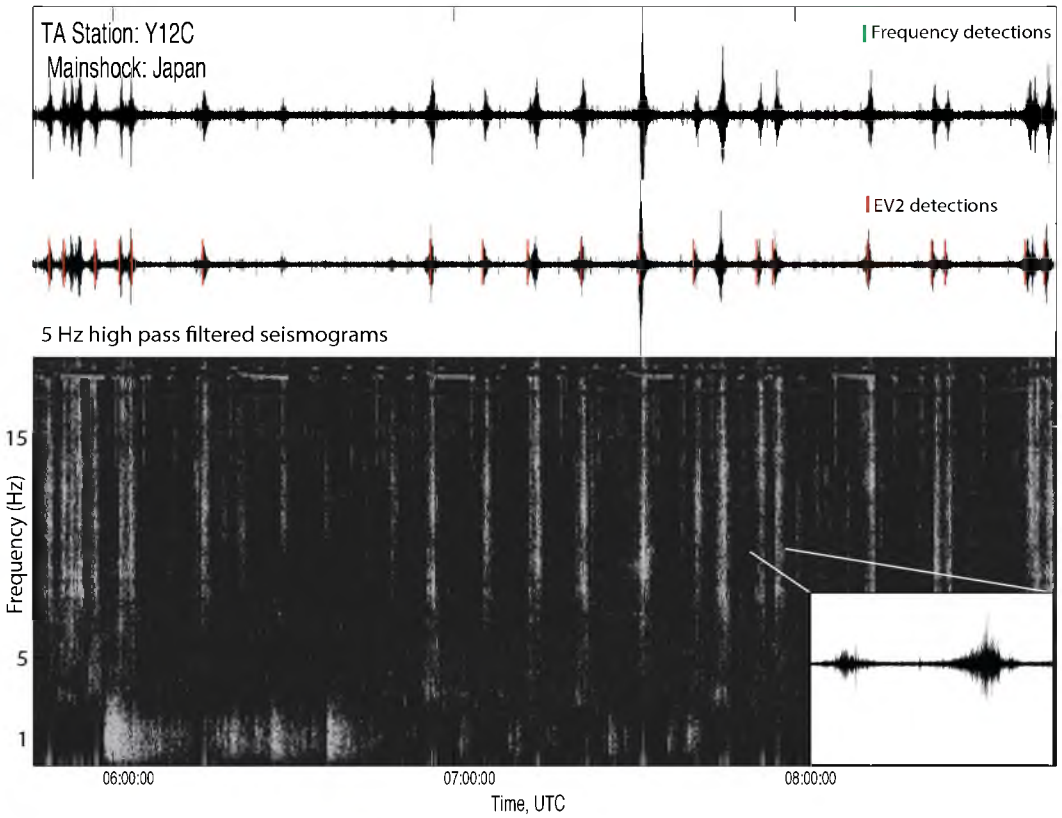

Figure 3.6 Spectral constraints for earthquake detection. Across TA, there are a number of semi-broadband noise sources that can be excluded from earthquake detections by requiring a minimum amount of signal in the 1-6 Hz range.

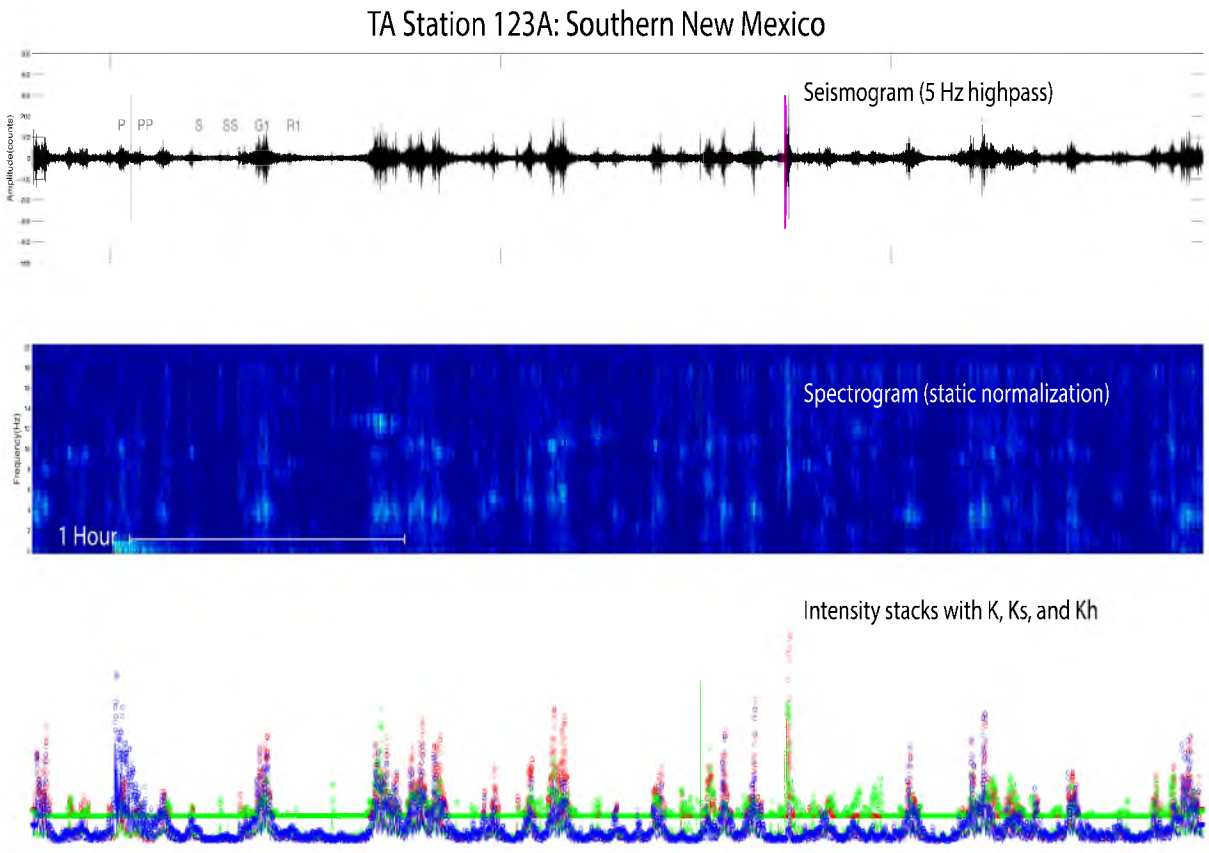

Figure 3.7 Frequency-domain picking on a noisy record in southern New Mexico. The magenta line (top panel) indicates where the frequency method is able to discriminate a small earthquake signal based on spectral character.

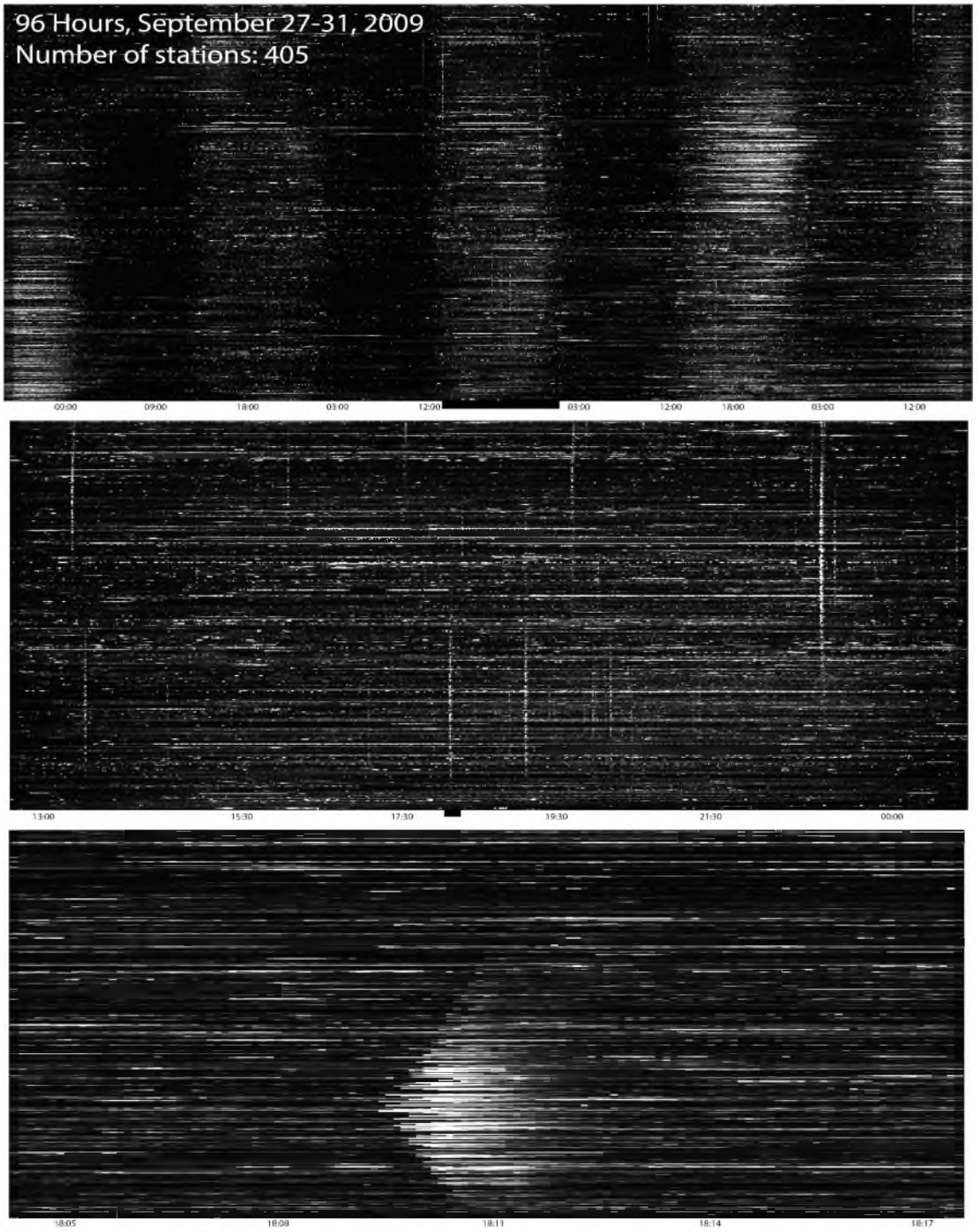

Figure 3.8 Frequency array method. Top: 4 days of energy distribution across the active array. Middle: 1 day (timing indicated by black bar on x-axis above). Bottom: several minutes of data around a magnitude 2 earthquake. The distance move-out makes it possible to discriminate as an earthquake source.The y-axis for each panel is the amplitude time series for each station, sorted by distance from the mainshock.

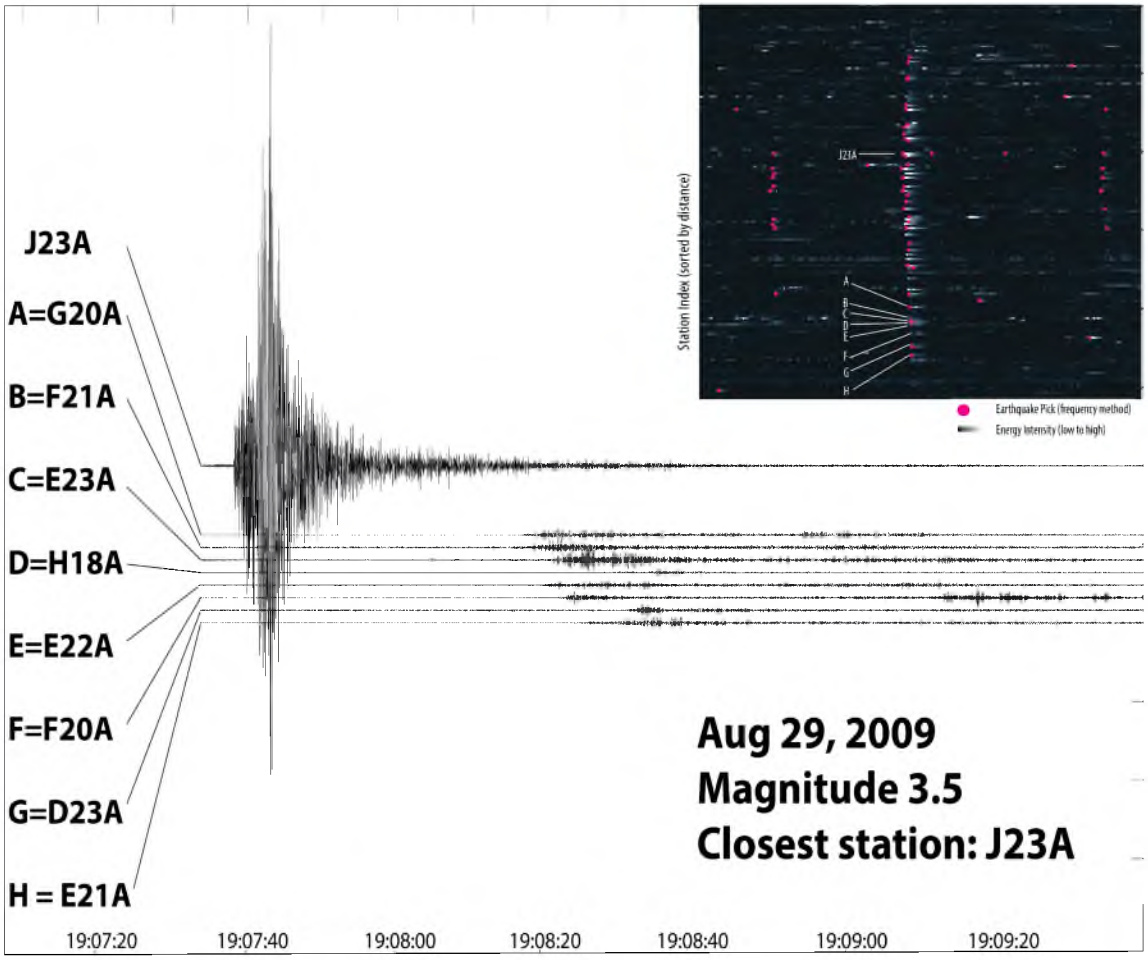

Figure 3.9 Frequency detection on a M3.5 earthquake in the Samoa, 2009 mainshock coda. Magenta circles indicate frequency detections. The number of stations with clearly visible coherent energy exceeds the number of stations that successfully capture a detection. There are three earthquakes in the inset panel. For the largest event, the middle, we show the farthest stations from the epicenter (nearest station J23A, distance between J23A and A-H > 300km).

CHAPTER 4

ALGORITHM IMPLEMENTATION ON A GLOBAL MAINSHOCK DATABASE

4.1 Which Mainshocks to Use

In order to identify instances of dynamic triggering across TA, we choose a database of mainshocks that exhibit the largest array averaged amplitudes between 2004-2013. There is some evidence to suggest that amplitude plays a role in the occurrence of dynamic triggering (Feltzer, 2006; Trugman, 2013; van der Elst & Brodsky, 2010; We et al., 2012). Alternatively, other researchers have concluded that amplitude is unlikely to be a dominant driver (Parsons et al., 2014). In the absence of clear catalysts in the literature, we chose to evaluate the most significant events that occurred during the TA deployment on the basis of surface wave amplitudes. Array averaged amplitudes for each mainshock were determined by first rotating the north and east channels of each seismogram into the radial (R) and transverse (T) components using the backazimuth to the mainshock. Next, the highest velocity for a segment of the record 3 hours following the mainshock origin time was picked for all three channels (R, T, and vertical (Z)) using SAC. For each station, the 20 largest R, T, and Z averages for all mainshocks were considered (Figure 4.1).

The TA reached > 200 stations starting in 2007. There were 5 events in the initial top 20 between 2004 and 2007. An additional 3 overlapped in time within a 2-day window. Choosing only the first of the overlapping sequences and excluding events thatoccurred without sufficient station coverage for the array visualization method results in a mainshock database containing 18 events covering a diverse range of geographic locations and source types (Figure 4.2). Most of the events are above magnitude 8. The remaining 7 events are from M7 or greater events that occurred relatively close to the array. For referencing below, each mainshock is referred to by its corresponding alphabetic character (Table 4.1).

4.2 Background Noise Levels Across TA

Before exploring the seismic response following a specific mainshock, it is useful to develop an understanding of the background signal across the array. We process each mainshock with the array method described above. The most obvious and ubiquitous signal that emerges is a clear diurnal variation in high frequency signal across the array. It is clear from Figure 4.3 that the increase in signal amplitude during daylight hours is a combination of uncorrelated anthropogenic activity and correlated signal from events related to extraction activities. This result is significant because for simple picking algorithms implemented across the TA, the pick rate is driven by noise (see section above). Furthermore, if we are able to develop a picker which successfully picks only signal (100% accuracy), relying on stationary background rates to determine rate increases will still lead to grossly inaccurate conclusions.

Understanding this, and that our frequency-domain algorithm identifies characteristically different noise than the EV2 detector, we make an effort to understand the effect of diurnal noise on the single-station picking algorithm outlined above (section 3.2). We verify our seismic event picks by a comparison for the active TA footprint with the ANF database; this tells us that the events we capture follow very closely to the reviewed events, and therefore, our databases likely vary only in the magnitudes we are able to recover (Figure 4.3). As expected, there are clear diurnal noise contributions above that can be attributed to pick rate increases, but are unrelated to event rate increases (Figure 4.4).

4.3 Calculating Significant Rate Increases (95 and 99% Confidence)

Rate increases are typically considered significant if they exhibit a sufficiently low probability of occurring randomly. To calculate the probability, we assume earthquakes follow a Poissonian distribution. In this distribution, events are assumed to occur at a constant rate. For this study, probabilities lower than 5% are considered. These values are based on the number of events within the postevent window as compared with a pre-event window (see below for discussion on window parameters). We define Npre as the number of events in the pre-event window of a specific duration (usually 2 days). Likewise, Npost is the equivalent window after the mainshock for the same duration. Therefore, for a Poissonian distribution:

$$\mu = \text{Npre}$$

$$\delta = \text{Npost}$$

and the standard deviation is calculated by:

$$\sigma = \sqrt{\mu} \tag{4.1}$$

Thus, Npost rates are significant at the 95% confidence level above 1.98 standard deviations (Taylor, 1982):

$$\delta \geq \mu + 1.98\,\sigma \tag{4.2}$$

and 99% rates are significant when:

$$\delta \geq \mu + 2.58\,\sigma \tag{4.3}$$

This is a typical method used in dynamic triggering studies (Velasco et al., 2008) and represents an approximation of the more robust binomial process (Pankow, et al., 2004). Although we recognize there are inherent complications (i.e., these are often small sample sets and therefore, significance is overestimated, and the method assumes a population of independent events that occur at a constant rate), we propose that this statistical approach is permissive of, although not sufficient evidence alone for, a significant rate increase linked to dynamic triggering.

4.4 Choosing Window Length

Time dependence in both the background noise rate and seismic event rate require that our observational windows either span whole day multiples, or that background rates are completely accounted for. The predictable result of relying on inappropriate windowing around the mainshock can be clearly illustrated by considering a 10-hour window that spans (+/- 5 hours) each mainshock. Observing event rates with these windows results in statistically significant rate increases for three events, G, N, and O (see Appendix). All three of these mainshocks have origin times in the early to mid-morning. The repercussion of having an origin time within this specific window is that

triggered rate increases will be indistinguishable from the large midday rate hike determined from ANF records for these regions. As a definitive illustration, if the equivalent 10-hour window is shifted by 24 hours to the day prior to the mainshock, event rate counts result in the same statistically significant increase in seismicity. Clearly, the timing of our windows matter.

4.5 Four Day Window (+/- 2 Days Around Mainshock)

To evaluate the occurrence of both instantaneous and delayed triggering up to 2 days, a 4-day window spanning the mainshock origin time is evaluated. To begin, the number of events is tallied separately for day and night. The mean daily rate for all included mainshocks is ~ 24 and the night rate is ~ 8. The ratio of day/night events increases to the east. There is no clear weekday/weekend trend for these data. Comparing total pre-event and postevent rates sheds light on any cases that may exhibit prolific or extended triggering at the 95% and 99% confidence levels. Because of the large difference in average number of events between the day and night, mainshocks which happen at night and induce earthquakes during the passage of their surface waves may do so at a significant level, but be obscured due to the large diurnal variation. This can happen because a significant night increase is still below the mean day rate. Therefore, bulk rate changes must be evaluated judiciously.

4.6 Instantaneous Triggering

In order to evaluate rate increases following the passage of surface waves for each event, we use a simple test. The test results in a TRUE outcome if the number of events

for the day or night window during which the passage of surface waves occurred exceeds the equivalent window minus 24 hours, by a significant level. No events meet the criteria at the 99% confidence level. One mainshock has a rate increases (Npre = 25, Npost = 39) at or above 95% confidence (Table 4.2.).

4.7 Delayed Triggering

Every mainshock has a related surface wave window that occurred either during the day or at night. Instantaneous triggering was determined using this initial window. To evaluate the occurrence of delayed dynamic triggering for each mainshock, we subject mainshocks A-P to two tests. The first test compares the day/night window following the instantaneous window. This test results in TRUE if either of these windows (comparison of day and night rates) results in a rate increase at or above the 95% confidence level. The second test is meant to assess both the robustness of the increase and identify protracted increases over the entire observational window (2 days). This second test simply sums the events that occurred during either daylight or nighttime hours and compares them with the number of events that happened during the hours corresponding to the same time of day before the mainshock. For the first test, event M is TRUE during the night and events B and N are TRUE during the day. For test two, N persists as TRUE during daylight hours (events G, M, and O are added at the 95% confidence level). Event B no longer passes. For night rates – M persist at the 99% confidence level (see Appendix for event counts).

4.8 Summary of Identified Dynamic Triggering

The events identified in sections 4.6 and 4.7 represent the maximum possible number of mainshocks that are likely to have caused triggering. A closer look at each potential mainshock is required to credibly report potential triggering based on spatio-temporal clustering. In the cases where instantaneous triggering is suspected, there are no demonstrated cases of widespread prolific triggering. The single event showing marginal increases in seismicity (95% confidence level) is event G, the 2009, Samoa event. In this case, the majority of the seismicity occurred in NE Wyoming with limited contributions from New Mexico and Colorado. All event increases were limited to daylight hours.

For delayed triggering, the nighttime rate increase following mainshock M offers strong evidence for a delayed effect with respect to the mainshock. This increase in events during the following night was sufficiently high to carry the rate increase at a significant level to pass the second test. The observational window for this mainshock is complicated because the postevent window includes two mainshocks greater than magnitude 8, and one magnitude 7 that occurred very close to the array margin (Baja California). Despite this, the seismicity response was very simple with nearly all events not related to Baja occurring in northern Arkansas. The waveform similarity of the Arkansas sequence indicates that all events have similar locations.

The remaining mainshock demonstrating evidence for delayed dynamic triggering for both tests is N. This is the Costa Rica, 2012 mainshock. Most potentially triggered events occur in regions of known surface or underground coal and iron extraction, including Marquette, MI, NW Alabama (coal), E Missouri (iron), and north central Tennessee (coal and metals). There is no evidence for nighttime rate increases. To

explore the temporal robustness of the rate increase for this mainshock, we evaluate ambient rate variation for a 12-day window, prior to the mainshock. We find event counts for the first 2 days after the mainshock (42 and 57 events) to be well within the natural variation (min:3, max:61) seen in the prior week. The large natural variation exceeds the rate increase determined significant. By this analysis, there is no legitimate basis for triggering from this mainshock.

The remaining three events that show an increase in event count are B, G, and O. B, in 2007, does so exclusively during the day. The highest number of events contributing to the rate increase is a group of off-array or array-border events between northern Mexico and southern Arizona near known surface copper mine operations. G events are predominantly in the active coal region of northeast Wyoming, as discussed earlier, and demonstrate no nighttime activity. The last event, O, in 2012, has daylight only increases, most occurring near active coal operations in eastern Kentucky.

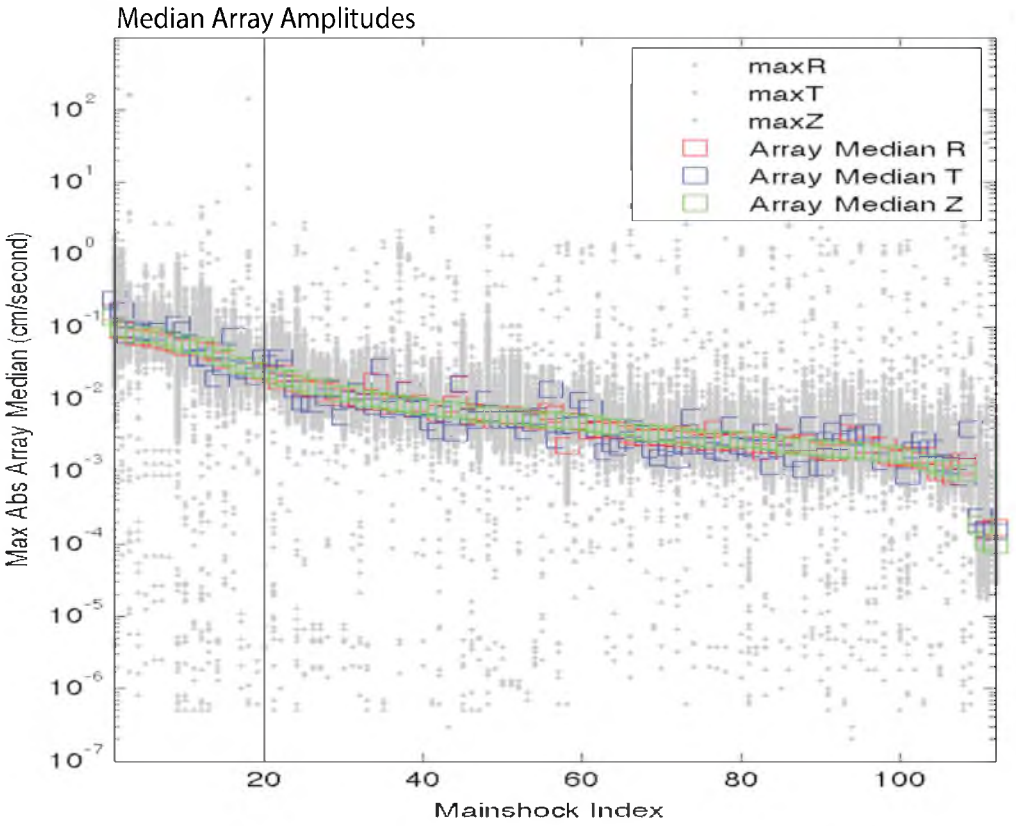

Figure 4.1 Median array amplitudes. A mainshock database was built by evaluating the 20 largest array averages for all earthquakes M > 7 that occurred during the deployment of TA (2004-2013). The vertical line indicates our cut-off for the top 20 events based on median array amplitudes for the radial, transverse, and vertical components.

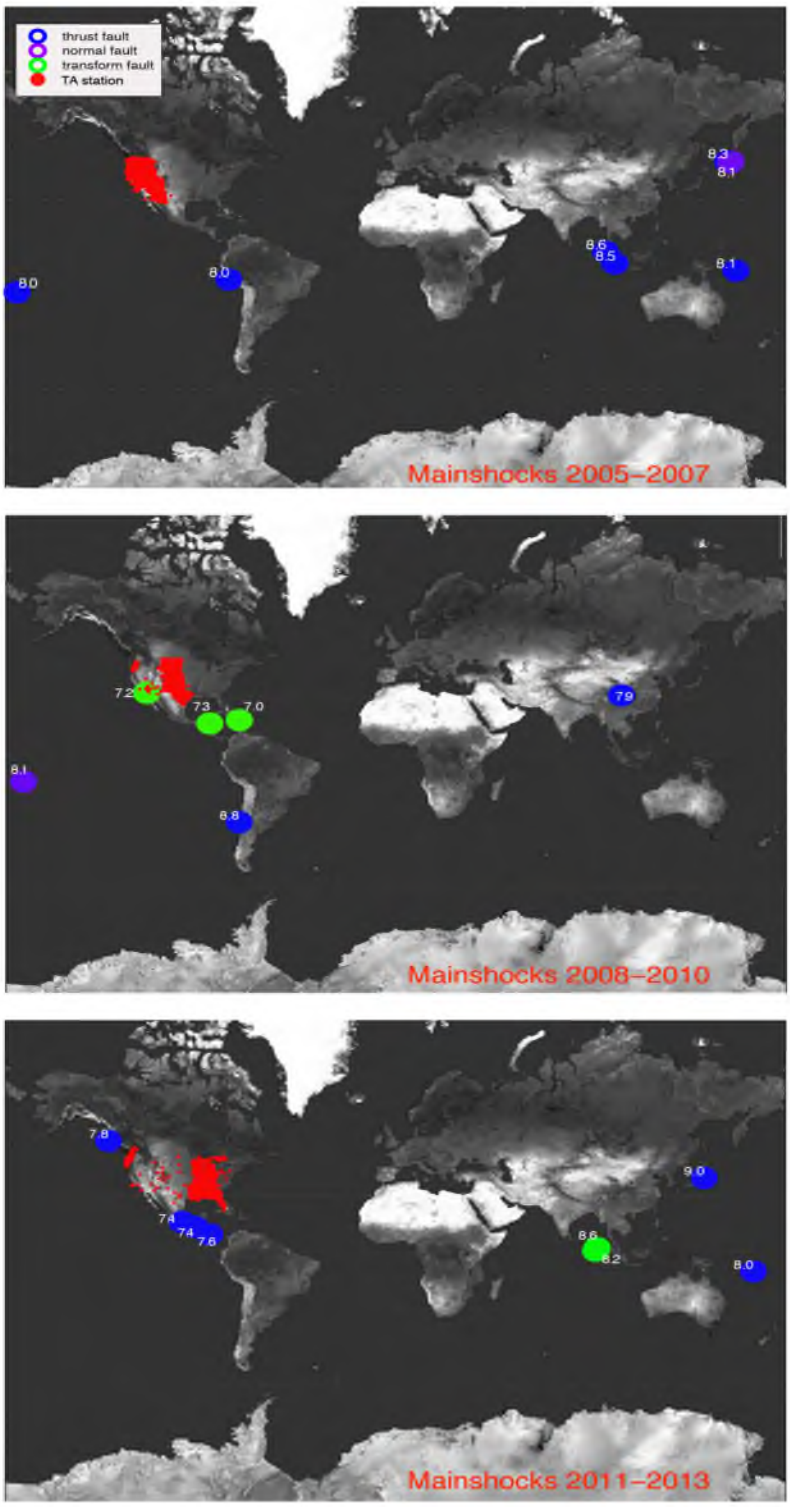

Figure 4.2 Mainshock database sorted by event type and year. Red dots indicate the active array locations for the first year of the time interval on each map.

Table 4.1 Mainshock date and magnitude. Ten events occurred during daylight hours (7am -7pm local time). Eight events occurred at night

Index	Date	Time	Magnitude
A	1/13/2007	4:23:21	8.1
B	4/1/2007	20:39:58	8.1
C	8/15/2007	23:40:37	8.0
D	9/12/2007	11:10:26	8.5
E	5/12/2008	6:28:01	7.9
F	5/28/2009	2:24:45	7.3
G	9/29/2009	17:48:10	8.1
H	1/12/2010	21:53:00	7.0
I	2/27/2010	6:34:14	8.8
J	4/4/2010	22:40:43	7.2
K	3/11/2011	5:46:23	9.0
L	3/20/2012	18:02:47	7.4
M	4/11/2012	8:38:37	8.6
N	4/11/2012	10:43:09	8.2
O	9/5/2012	14:42:00	7.6
P	11/7/2012	16:35:47	7.4
Q	10/28/2012	3:04:08	7.8
R	2/6/2013	1:12:27	8.0
S	4/12/2012	7:15:48	7.0

*Day
**Night

Table 4.2 Instantaneous triggering showing event counts for Npre and Npost windows. See text for discussion on the potential triggering indicated by the gray shading. Blue boxes indicate the mainshock happened during local nighttime hours (7:00 pm – 7:00 am)

Mainshock	Ordinal Day/Year	mu or Npre	sqrt(mu) or standard deviation	number counted or Npost	95% Threshold (assume Gaussian)	99% Threshold (assume Gaussian)	Pass/Fail	Pass/Fail
a*	132007	4	2.00	6	8.00	10.00	FALSE	FALSE
b**	912007	14	3.74	16	21.48	25.22	FALSE	FALSE
c	2272007	5	2.24	8	9.47	11.71	FALSE	FALSE
d	2552007	11	3.32	12	17.63	20.95	FALSE	FALSE
e	1332008	23	4.80	18	32.59	37.39	FALSE	FALSE
f	1482009	7	2.65	3	12.29	14.94	FALSE	FALSE
g	2722009	25	5.00	39	35.00	40.00	95	FALSE
h	122010	38	6.16	37	50.33	56.49	FALSE	FALSE
i	582010	11	3.32	6	17.63	20.95	FALSE	FALSE
j	942010	23	4.80	21	32.59	37.39	FALSE	FALSE
k	702011	31	5.57	19	42.14	47.70	FALSE	FALSE
l	802012	23	4.80	26	32.59	37.39	FALSE	FALSE
m	1022012	2	1.41	3	4.83	6.24	FALSE	FALSE
n	2492012	31	5.57	42	42.14	47.70	FALSE	FALSE
o	3122012	26	5.10	32	36.20	41.30	FALSE	FALSE
p	3022012	9	3.00	5	15.00	18.00	FALSE	FALSE

*Night
**Day

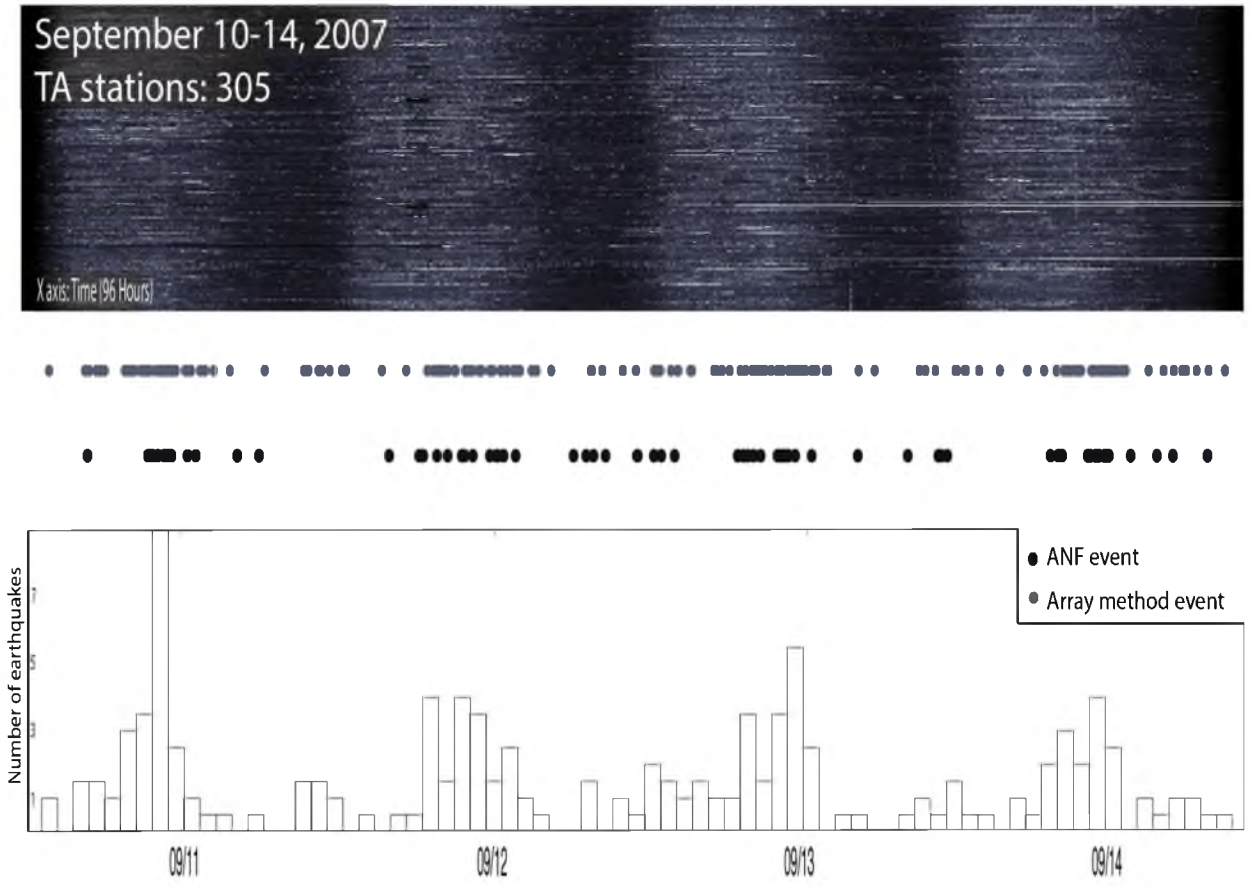

Figure 4.3 Energy distribution for 4 days of data from 305 active stations spanning the September, 2007 mainshock (top) compared with event counts from the frequency array method (grey) and the ANF database (black) for events within the active TA footprint. The histogram is from our frequency array event database and indicates that event increases are temporally coincident with daylight noise increases (lighter vertical bars, top panel). The x-axis for all panels is the same.

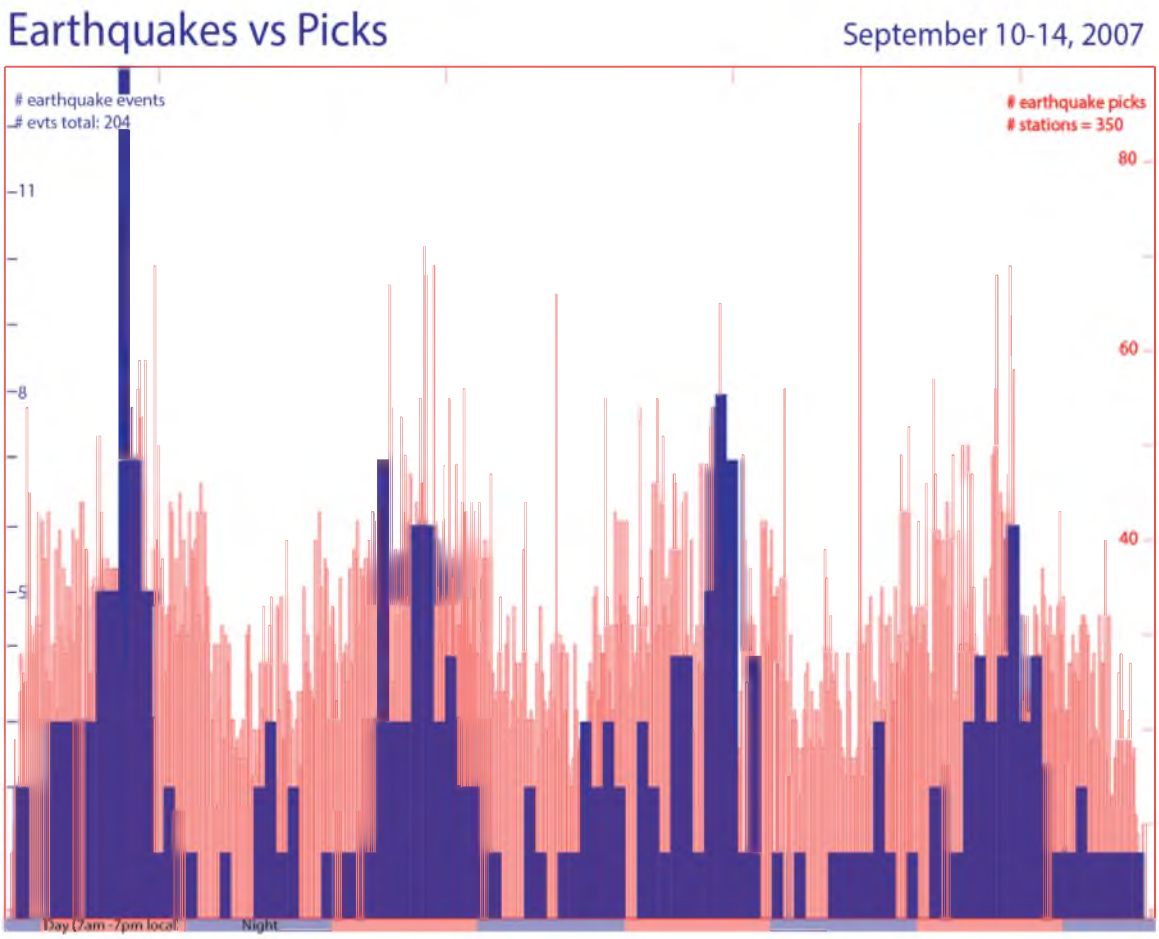

Figure 4.4 Earthquake vs. pick count. Earthquake distribution is nonstationary for windows > 1 day. It is also apparent that morning event rates differ from midday event rates (which are by far the highest) or early evening event rates. Because pick counts do not mirror earthquakes, there is clearly an effect from diurnal, nonearthquake noise sources for pick databases.

CHAPTER 5

DISCUSSION

5.1 Background Rates

One of the major accomplishments of this study has been the development of an efficient tool with which we are able to evaluate ambient seismic noise conditions across the array. Published analysis of ANF catalogs give us an idea of the variation in background seismicity, while IRIS quality assurance products, power spectral density (PSD) plots specifically, confirm the persistence of diurnal noise patterns. Our method merges these disparate observations and offers rapid visualization of the ambient noise and correlated signal across the array. This capacity is vital for triggering studies intending to use the TA data, and specifically single-station methods, because understanding the variation in background event rates and noise contributions is a vital part of interpreting seismicity rate changes at any given time. A clear understanding of the variation in these two parameters, background noise and background events, is the foundation for dynamic triggering studies reliant on these data.

One unforeseen insight gained from the ability to view transient signal distributions across the array is that there exists a host of secondary signals that hint at real earth processes previously uncharacterized, but present, in seismic data. We observed

this by looking at signal within frequency bands specifically meant to highlight local earthquakes. In general, however, the direct spectroscopic tuning inherent in the method make it a valuable tool for systematic search of any number of these band-limited phenomena.

To relate these findings to broader single-station dynamic triggering studies, it is useful to highlight conditions specific to TA. In general, seismic stations are carefully sited to avoid signal contamination related to the hours and activities of productive societies. This is a luxury that low density, long-term arrangements can afford. TA, conversely, has very specific spacing (70 km) and timing constraints, specifically those related to the practicality of permitting and installing 400 serviceable stations whose residence time will be 2 years. Practically speaking, this means that TA stations are not sited on bedrock, or typically very far from inhabited residence. As a result, the sites are easily accessible and remain safely in the care of specific property owners for the duration of their installment. The tradeoff is in the higher frequency bands where dynamic triggering studies necessarily probe; these bands are highly contaminated in a nonstationary way. Some of this contamination may represent signal content from unknown sources that will offer future insight into solid earth-atmospheric coupling, for example. As a whole though, these energy sources represent significant interpretational barriers for both STA/LTA and frequency-domain detection algorithms.

5.2 On the Found Instances of Dynamic Triggering

The mainshock database compiled for this study provided us with the most likely global events to trigger seismicity rate increases in the U.S. based on the premise of

amplitude as a driver. Temporal distribution and coherent station spacing allowed repeat sampling of sections of the crust to levels of scrutiny rarely before accomplished on this scale. Despite this, clear cases of instantaneous dynamic triggering are absent, and cases of delayed triggering are relatively rare. When present, these cases almost exclusively occur for daylight-only seismicity (areas that are seismically prolific during the day and comparatively silent at night). The one exception to this is the night rate increase following the Sumatra, 2012 8.6 and 8.2 events. N7otably, this sequence occurred as a set of repeating events centered in central Arkansas suggestively near active coal operations.

Daylight-only events are problematic within the context of dynamic triggering because their occurrence can be largely independent of the ambient stress state. Therefore, one logical conclusion would be that these rate changes directly reflect the daily operations of extraction related industry in those areas. This conclusion gains traction from the observation that typical weekly variation in event rates can be significantly greater than within the subwindows under observation. It is further supported by the absence of any increase in nighttime activity within these same areas after daytime rate increases are detected. It is nonphysical to assume that tectonic strain release would behave this way. Considering the demonstrated lack of understanding regarding rate changes as part of weekly or even quarterly cycles, it is hard to maintain a solid claim for rate increase during daylight hours for any of the mainshocks observed here. Another interpretation is that human industrial activity alters the local state of stress in a way that increases sensitivity to small (.02 cm/s and above) stress perturbations. This second case is reasonable only for subsurface operations. Because within the resolution of our locations, it is possible to make a general correlation with both known surface and

underground extraction operations for nearly every potentially triggered site, it is difficult to carry this conclusion further. In the end, the Sumatra 2012 sequence, which contained three qualifying mainshocks within our amplitude cut-off in the postevent window, was the only mainshock demonstrating modest evidence for potential triggering. This potential triggering is limited to one source area, lasts for several hours, and is not invigorated, or even present within the surface waves of any of the three large mainshocks that occur during the observation window.

CHAPTER 6

CONCLUSION

6.1 Summary of Conclusions

The development of a frequency-domain detection algorithm is based on the concept that band-limited contributions to earthquake detections can be minimized using the STA/LTA concept from traditional time-domain algorithms while encoding specific spectral information into the amplitude time-series. We pass our STA/LTA picker over three separate band limits, requiring that it meet all three criteria to signal a detection. It is then subject to additional criteria, which requires it to possess characteristics of a real earthquake, such as adherence to typical decay envelops and limited signal duration. While this method increases the accuracy of earthquake detection databases compared to highly tuned STA/LTA algorithms in the time-domain, false detections are still the dominant constituent of these databases. This method may represent a useful tool for earthquake picking as implemented on long-term regional networks. Although this avenue is unexplored in the material above, the observation that the characteristic noise picked by this method is greater across the TA due to typical station siting than seen on other regional networks gives this idea promise.

For this study, in order to diagnose the crustal response to energy transients, we capitalize on the station density and uniform coverage in previously under-sampled regions that are unique to the TA dataset. Further development of the frequency detection method to include array-wide signal visualizations provides a framework wherein earthquake detections can be made at levels comparable to single-station detection methods, but with virtually no noise contributions. This provides a robust framework wherein the occurrence of dynamic triggering following the largest earthquakes affecting the crust during the occupation of the TA can be evaluated.

From this, we find that the 18 largest earthquakes based on surface wave amplitude across TA, and therefore the group most likely to trigger far-field aftershocks based on amplitude as a driver, show almost no evidence of dynamic triggering either instantaneously with the passage of the highest amplitude surface waves, or within 2 days following the mainshock. The limited evidence for rate increases is restricted to daylight hours, except in the case of the Sumatra event, which affected seismicity at night, at a site specifically known for earthquakes driven by anthropogenic influence (fluid injection or extraction related seismicity). This evidence suggests that either extraction/injection sites are more sensitive to small earthquake transients, or that our ability to accurately parameterize rate increases is limited based on a lack of information regarding the anthropogenic patterns at these specific sites, i.e., weekend and weekday well site practices. Overall, we note a conspicuous lack of dynamic triggering for most cases explored.

We conclude that dynamic triggering is unambiguously rare for both large and small magnitude earthquakes (as small as is typically recovered by human analysts).

Furthermore, locations that correspond to significant increases in seismicity following global mainshocks occur without exception in regions considered "active" because there is a history of significant tectonic activity at that site, or industrial or energy sector activities generate consistent seismic energy there. We conclude that dynamic triggering is a limited phenomenon requiring highly specific conditions (phases, orientations, duration of shaking, in addition to amplitude) and/or that amplitude is not a viable driver for these far-field processes at the amplitudes observed in this study.

6.2 Future Work

One of the most significant limitations to the frequency array method developed above is that it requires an analyst to review the array image. When the total image contains a relatively short time (< 5 hours), manual processing is trivial because determining event counts, locations, and times is a rapid exercise. In general, window length is proportional to processing time, and inversely proportional to accuracy. This effort also scales with computing resources. For a 4-day record, this processing reaches a reasonable upper limit for computing resources and analyst patience (Matlab on a 3.4 GHz i7 assuming ample available memory and maximized Java heap allocations).

To ensure an event database is populated by true events, an event associator, or binding algorithm, is required. These algorithms associate related picks into legitimate events while discarding uncorrelated noise. We accomplish this by eye with our frequency array method, and although unsophisticated, it is an efficient and accurate way to process small datasets. However, we now know that background rates are the most important part of understanding rate increases, and longer time windows than can be

comfortably processed manually are required to fully characterize these rates for a given site.

Making associations between picks requires some form of spatio-temporal clustering. Picks from single-station detections by design yield the necessary parameters to accomplish this (latitude, longitude, and time). Therefore, finding earthquakes within a pick cloud should reasonably be a matter of parameterizing a density function for this purpose. Preliminary temporal clustering suggests this method will be highly successful at filtering out uncorrelated picks.

This increased level of automation can greatly enhance the value of the resultant databases because they can be populated with events to be evaluated objectively based on a users desired resolution (up to the minute scale) for any window. Statistically, this can have much greater potency than the analysis performed above. However, the price of binding programs is often resolution. By requiring a minimum number of stations, you limit the minimum recoverable event size. In the analysis above, we circumvent this issue by observing that signal distribution patterns are far more telling than binary picks, and therefore, it is possible to capture related seismic energy to a level nearly comparable to single-station detection. Reliance on a pick database to determine detections will require more robust quantification and analysis of recoverable magnitudes and false detection rates for single-station detections in the future.

APPENDIX

Earthquake event counts for pre- and postevent windows

Mainshock	Ordinal Day/Year	mu or Npre	sqrt(mu) or standard deviation	number counted or Npost	95% Threshold (assume Gaussian mu >9)	99% Threshold (assume Gaussian mu > 9)	Pass/Fail	Pass/Fail
a	132007	5	2.24	5	9.47	11.71	FALSE	FALSE
b	912007	5	2.24	3	9.47	11.71	FALSE	FALSE
c	2272007	23	4.80	1	32.59	37.39	FALSE	FALSE
d	2552007	5	2.24	9	9.47	11.71	FALSE	FALSE
e	1332008	6	2.45	6	10.90	13.35	FALSE	FALSE
f	1482009	2	1.41	0	4.83	6.24	FALSE	FALSE
g	2722009	9	3.00	23	15.00	18.00	95	99
h	122010	26	5.10	12	36.20	41.30	FALSE	FALSE
i	582010	2	1.41	4	4.83	6.24	FALSE	FALSE
j	942010	11	3.32	3	17.63	20.95	FALSE	FALSE
k	702011	5	2.24	9	9.47	11.71	FALSE	FALSE
l	802012	14	3.74	13	21.48	25.22	FALSE	FALSE
m	1022012	2	1.41	0	4.83	6.24	FALSE	FALSE
n	2492012	9	3.00	27	15.00	18.00	95	99
o	3122012	8	2.83	26	13.66	16.49	95	99
p	3022012	1	1.00	2	3.00	4.00	FALSE	FALSE
rates for 10 hour window (+/- 5 hours around mainshock)								99
a	132007	5	2.24	9	9.43	10.77	FALSE	FALSE
b	912007	15	3.87	9	22.75	26.62	FALSE	FALSE
c	2272007	5	2.24	7	9.47	11.71	FALSE	FALSE
d	2552007	6	2.45	9	10.90	13.35	FALSE	FALSE
e	1332008	23	4.80	19	32.59	37.39	FALSE	FALSE
f	1482009	7	2.65	6	12.29	14.94	FALSE	FALSE
g	2722009	12	3.46	6	18.93	22.39	FALSE	FALSE
h	122010	13	3.61	12	20.21	23.82	FALSE	FALSE
i	582010	11	3.32	4	17.63	20.95	FALSE	FALSE
j	942010	6	2.45	7	10.90	13.35	FALSE	FALSE
k	702011	31	5.57	11	42.14	47.70	FALSE	FALSE
l	802012	4	2.00	1	8.00	10.00	FALSE	FALSE
m	1022012	1	1.00	17	3.00	4.00	95	99
n	2492012	2	1.41	3	4.83	6.24	FALSE	FALSE
o	3122012	3	1.73	5	6.46	8.20	FALSE	FALSE
p	3022012	9	3.00	5	15.00	18.00	FALSE	FALSE
rates for nighttime windows (avg night rate before mainshock and night of or after)								
a	132007	12	3.46	8	18.93	22.39	FALSE	FALSE
b	912007	14	3.74	26	21.48	25.22	95	99
c	2272007	25	5.00	22	35.00	40.00	FALSE	FALSE
d	2552007	30	5.48	37	40.95	46.43	FALSE	FALSE
e	1332008	23	4.80	29	32.59	37.39	FALSE	FALSE
f	1482009	33	5.74	29	44.49	50.23	FALSE	FALSE
g	2722009	25	5.00	31	35.00	40.00	FALSE	FALSE
h	122010	38	6.16	47	50.33	56.49	FALSE	FALSE
i	582010	36	6.00	28	48.00	54.00	FALSE	FALSE
j	942010	23	4.80	23	32.59	37.39	FALSE	FALSE
k	702011	30	5.48	24	40.95	46.43	FALSE	FALSE
l	802012	23	4.80	22	32.59	37.39	FALSE	FALSE
m	1022012	12	3.46	14	18.93	22.39	FALSE	FALSE
n	2492012	31	5.57	57	42.14	47.70	95	99
o	3122012	26	5.10	20	36.20	41.30	FALSE	FALSE
p	3022012	4	2.00	5	8.00	10.00	FALSE	FALSE
rates for day window (avg day rate before and day of or after)								

Earthquake event counts for pre- and postevent windows continued

Mainshock	Ordinal Day/Year	mu or Npre	sqrt(mu) or standard deviation	number counted or Npost	95% Threshold (assume Gaussian mu >9)	99% Threshold (assume Gaussian mu > 9)	Pass/Fail	Pass/Fail
a	132007	26	5.10	18	36.20	41.30	FALSE	FALSE
b	912007	24	4.90	32	33.80	38.70	FALSE	FALSE
c	2272007	54	7.35	44	68.70	76.05	FALSE	FALSE
d	2552007	54	7.35	62	68.70	76.05	FALSE	FALSE
e	1332008	50	7.07	61	64.14	71.21	FALSE	FALSE
f	1482009	60	7.75	57	75.49	83.24	FALSE	FALSE
g	2722009	52	7.21	72	66.42	73.63	95	FALSE
h	122010	64	8.00	78	80.00	88.00	FALSE	FALSE
i	582010	59	7.68	35	74.36	82.04	FALSE	FALSE
j	942010	47	6.86	52	60.71	67.57	FALSE	FALSE
k	702011	59	7.68	46	74.36	82.04	FALSE	FALSE
l	802012	39	6.24	46	51.49	57.73	FALSE	FALSE
m	1022012	19	4.36	29	27.72	32.08	95	FALSE
n	2492012	42	6.48	90	54.96	61.44	95	99
o	3122012	43	6.56	57	56.11	62.67	95	FALSE
p	3022012	60	7.75	40	75.49	83.24	FALSE	FALSE
day time rates for 4 day window (all day events pre vs all day events post)								
		mu or Npre	sqrt(mu) or standard deviation	number counted or Npost	95% Threshold (assume Gaussian mu >9)	99% Threshold (assume Gaussian mu > 9)		
a	132007	12	3.46	13	18.93	22.39	FALSE	FALSE
b	912007	22	4.69	22	31.38	36.07	FALSE	FALSE
c	2272007	15	3.87	15	22.75	26.62	FALSE	FALSE
d	2552007	14	3.74	20	21.48	25.22	FALSE	FALSE
e	1332008	34	5.83	27	45.66	51.49	FALSE	FALSE
f	1482009	11	3.32	9	17.63	20.95	FALSE	FALSE
g	2722009	20	4.47	10	28.94	33.42	FALSE	FALSE
h	122010	22	4.69	21	31.38	36.07	FALSE	FALSE
i	582010	15	3.87	11	22.75	26.62	FALSE	FALSE
j	942010	12	3.46	12	18.93	22.39	FALSE	FALSE
k	702011	44	6.63	28	57.27	63.90	FALSE	FALSE
l	802012	11	3.32	8	17.63	20.95	FALSE	FALSE
m	1022012	6	2.45	19	10.90	13.35	95	99
n	2492012	4	2.00	3	8.00	10.00	FALSE	FALSE
o	3122012	6	2.45	7	10.90	13.35	FALSE	FALSE
p	3022012	8	2.83	11	13.66	16.49	FALSE	FALSE
night time rates for 4 day window (all night events pre vs all nightevents post)								

REFERENCES

Allen, R. V. (1978). Automatic earthquake recognition and timing from single traces. *Bulletin of the Seismological Society of America, 68*(5), 1521-1531

Astiz, L., Eakins, J.A., Martynov, V.G., Cox, T.A., Tytell, J., Reyes, J.C., Newman, R.L., et al. (2013). The array network facilitiy seismic bulletin: Products and an unbiased view of United States seismicity. *Seismological Research Letters*, *85*, 576-593

Brodsky, E. E. (2006). Long-range triggered earthquakes that continue after the wave train passes. *Geophysical Research Letters, 33*(15), 5-5, L15313

Brodsky, E.E., & Prejean, S.G. (2005). New constraints on mechanisms of remotely triggered seismicity at Long Valley Caldera, *Journal of Geophysical Research*, *110*, B04302

Brodsky, E. E., Roeloffs, E., Woodcock, D., Gall, I., & Manga, M. (2003). A mechanism for sustained groundwater pressure changes induced by distant earthquakes. *Journal of Geophysical Research, 108*, 10

Belardinelli, M. E., Bizzarri, A., & Cocco, M. (2003). Earthquake triggering by static and dynamic stress changes. *Journal of Geophysical Research, 108*, 16

Feltzer, K. R., & Brodsky, E. E. (2006). Decay of aftershock density with distance indicates triggering by dynamic stress. *Nature (London), 441*(7094), 735-738. doi:http://dx.doi.org/10.1038/nature04799

Freed, A. M. (2005). Earthquake triggering by static, dynamic, and postseismic stress transfer. *Annual Review of Earth and Planetary Sciences, 33*, 335-367. doi:http://dx.doi.org/10.1146/annurev.earth.33.092203.122505

Freed A.M., Lin J. (2001). Delayed triggering of the 1999 Hector Mine earthquake by viscoelastic stress transfer. *Nature, 411*,180–83

Gomberg, J., & Sherrod, B. (2014). Crustal earthquake triggering by modern great earthquakes on subduction zone thrusts. *Journal of Geophysical Research, Solid Earth, 119*,1235–1250, doi:10.1002/2012JB009826.

Gomberg, J., Bodin, P., Larson, K., & Dragert, H. (2004). The fundamental process of

earthquake nucleation by transient deformations revealed by the M7.9 Denali, Alaska earthquake. *Nature, 427*, 621-624.

Gomberg, J., Reasenberg, P. A., Bodin, P., & Harris, R. A. (2001). Earthquake triggering by seismic waves following the landers and hector mine earthquakes. *Nature, 411*(6836), 462-466. doi:http://dx.doi.org/10.1038/35078053

Gonzalez-Huizar, H., & Velasco, A. A. (2011). Dynamic triggering; stress modeling and a case study. *Journal of Geophysical Research, 116*, 0-Citation B02304 doi:http://dx.doi.org/10.1029/2009JB007000

Heinzel, G., Rüdiger, A., Schilling, R., & Hannover, T. (2002). Spectrum and spectral density estimation by the Discrete Fourier transform (DFT), including a comprehensive list of window functions and some new flat-top windows. *Max Plank Institute*, *12*, 122.

Hill, D. P. (2008). Dynamic stresses, coulomb failure, and remote triggering. *Bulletin of the Seismological Society of America, 98*(1), 66-92 doi:http://dx.doi.org/10.1785/0120070049

Hill, D. P., Reasenberg, P. A., Michael, A. J., Arabasz, W. J., Beroza, G. C., Brumbaugh, D. S., & Zollweg, J. E. (1993). Seismicity remotely triggered by the magnitude 7.3 landers, California, earthquake. *Science, 260*(5114), 1617-1623

Hough, S. E. (2007). Remotely triggered earthquakes following moderate main shocks. *Special Paper - Geological Society of America, 425*, 73-86. doi:http://dx.doi.org/10.1130/2007.2425

Husker, A.L., & Brodsky E.E. (2004). Seismicity in Idaho and Montana triggered by the Denali Fault earthquake; a window into the geologic context for seismic triggering (in The 2002 Denali Fault earthquake sequence). *Bulletin of the Seismological Society of America, 94*(6, Part B*)*, 310-316

Johnson, P. A., & Jia, X. (2005). Nonlinear dynamics, granular media and dynamic earthquake triggering. *Nature (London), 437*(7060), 871-874 doi:http://dx.doi.org/10.1038/nature04015

Johnston, M. J. S., Prejean, S. G., & Hill, D. P. (2004). Triggered deformation and seismic activity under mammoth mountain in long valley caldera by the 3 November 2002 M (sub w) 7.9 Denali fault earthquake. *Bulletin of the Seismological Society of America, 94*(6), 360-369

Jugla, E. A. (2011). Delayed dynamic triggering of earthquakes; evidence from a statistical model of seismicity. *Europhysics Letters, 93*(1), 0-paper 19001. doi:http://dx.doi.org/10.1209/0295-5075/93/19001

Leys, C., Ley C., Klein, O., Bernard, P., & Licata, L. (2013). Detecting outliers: Do not use standard deviation around the mean, use absolute deviation around the median. *Journal of Experimental Social Psychology, 49*, 764-766

Manga, M., & Brodsky, E. (2006). Seismic triggering of eruptions in the far field; volcanoes and geysers. *Annual Review of Earth and Planetary Sciences, 34*, 263-291. doi:http://dx.doi.org/10.1146/annurev.earth.34.031405.125125

Matthews, M. V., & P. A. Reasenberg., (1988). Statistical methods for investigating quiescence and other temporal seismicity patterns. *Pure and Applied Geophysics,126*, 357–372

Moran, S. C., Power, J. A., Stihler, S. D., Sanchez, J. J., & Caplan-Auerbach, J. (2004). Earthquake triggering at Alaska volcanoes following the 3 November 2002 Denali fault earthquake. *Bulletin of the Seismological Society of America, 94*(6), 300-309

Pankow, K. L., Arabasz, W. J., Pechmann, J. C., & Nava, S. J. (2004). Triggered seismicity in Utah from the 3 November 2002 Denali fault earthquake. *Bulletin of the Seismological Society of America, 94*(6), 332-347

Parsons, T. (2005). A hypothesis for delayed dynamic earthquake triggering. *Geophysical Research Letters, 32(4)*, 4

Parsons, T., Segou, M., & Marzocchi, W. (2014). Invited Review: The global aftershock zone. *Tectonophysics, 618*, 1-34, doi: 10.1016/j.tecto.2014.01.038

Parsons, T., Kaven, J. O., Velasco, A. A., & Gonzalez-Huizar, H. (2012). Unraveling the apparent magnitude threshold of remote earthquake triggering using full wavefield surface wave simulation. *Geochemistry, Geophysics, Geosystems - G3, 13*(6), 0-Q06016. doi:http://dx.doi.org/10.1029/2012GC004164

Parsons, T., & Velasco, A. A. (2011). Absence of remotely triggered large earthquakes beyond the mainshock region. *Nature Geoscience, 4*(5), 312-316

Pollitz, F. F., Stein, R. S., Sevilgen, V., & Burgmann, R. (2012). The 11 April 2012 east Indian Ocean earthquake triggered large aftershocks worldwide. *Nature (London), 490*(7419), 250-253. doi:http://dx.doi.org/10.1038/nature11504

Prejean, S. G., Hill, D. P., Brodsky, E. E., Hough, S. E., Johnston, M. J. S., Malone, S. D., Oppenheimer, D. H., Pitt, A. M., & Richards-Dinger, K. B. (2004). Remotely triggered seismicity on the United States west coast following the Mw 7.9 Denali Fault earthquake. *Bulletin of the Seismological Society of America, 94*, S348-S359

Ripley, Brian D. (1989). Robust statistics — how not to reject outliers. I. Basic Concepts. *Analyst, 114*, 1693-1697

Shelly, D. R., Peng, Z., Hill, D. P., & Aiken, C. (2011). Triggered creep as a possible

mechanism for delayed dynamic triggering of tremor and earthquakes. *Nature Geoscience, 4*(6), 384-388. doi:http://dx.doi.org/10.1038/ngeo1141

Taylor, J. R. (1982). *An introduction to error analysis: The study of uncertainties in physical measurements* (2nd ed). Sausalito, CA: University Science Books

Trugman, D. T., Daub, E. G., Guyer, R. A., & Johnson, P. A. (2013). Modeling dynamic triggering of tectonic tremor using a brittle-ductile friction model. *Geophysical Research Letters, 40*(19), 5075-5079. doi:http://dx.doi.org/10.1002/grl.50981

Van der Elst, N.,J., & Brodsky, E. E. (2010). Connecting near-field and far-field earthquake triggering to dynamic strain. *Journal of Geophysical Research, 115*, 0-Citation B07311. doi:http://dx.doi.org/10.1029/2009JB006681

West, M. E., Sanchez, J. J., McNutt, S. R., Anderson, J. G., & von Seggern, D. (2005). Periodically triggered seismic events at Mt. Wrangell volcano following the Sumatra Andaman Islands earthquake. *Seismological Research Letters, 76*(2), 221.

Wu, J., Peng, Z., Wang, W., Gong, X., Chen, Q., & Wu, C. (2012). Comparisons of dynamic triggering near Beijing, China following recent large earthquakes in Sumatra. *Geophysical Research Letters, 39*(21)

Velasco, A. A., Hernandez, S., Parsons, T., & Pankow, K. (2008). Global ubiquity of dynamic earthquake triggering. *Nature Geoscience, 1*(6), 375-379. doi:http://dx.doi.org/10.1038/ngeo204